ARL
US Army Research Laboratory

Nonlinear Phase Field Theory for Fracture and Twinning with Analysis of Simple Shear

by JD Clayton and J Knap

NOTICES

Disclaimers

The findings in this report are not to be construed as an official Department of the Army position unless so designated by other authorized documents.

Citation of manufacturer's or trade names does not constitute an official endorsement or approval of the use thereof.

Destroy this report when it is no longer needed. Do not return it to the originator.

ARL

US Army Research Laboratory

Nonlinear Phase Field Theory for Fracture and Twinning with Analysis of Simple Shear

by JD Clayton
Weapons and Materials Research Directorate, ARL

J Knap
Computational and Information Sciences Directorate, ARL

1. REPORT DATE (DD-MM-YYYY)	2. REPORT TYPE	3. DATES COVERED (From - To)
September 2015	Reprint	15 May 2014–20 July 2015

4. TITLE AND SUBTITLE	5a. CONTRACT NUMBER
Nonlinear Phase Field Theory for Fracture and Twinning with Analysis of Simple Shear	
	5b. GRANT NUMBER
	5c. PROGRAM ELEMENT NUMBER
6. AUTHOR(S)	5d. PROJECT NUMBER
JD Clayton and J Knap	
	5e. TASK NUMBER
	5f. WORK UNIT NUMBER

7. PERFORMING ORGANIZATION NAME(S) AND ADDRESS(ES)	8. PERFORMING ORGANIZATION REPORT NUMBER
US Army Research Laboratory ATTN: RDRL-WMP-C Aberdeen Proving Ground, MD 21005-5069	ARL-RP-0546

9. SPONSORING/MONITORING AGENCY NAME(S) AND ADDRESS(ES)	10. SPONSOR/MONITOR'S ACRONYM(S)
	11. SPONSOR/MONITOR'S REPORT NUMBER(S)

12. DISTRIBUTION/AVAILABILITY STATEMENT
Approved for public release; distribution is unlimited.

13. SUPPLEMENTARY NOTES
Reprinted from Philosophical Magazine. 2015;95(24):2661–2696.

14. ABSTRACT
A phase field theory for coupled twinning and fracture in single crystal domains is developed. Distinct order parameters denote twinned and fractured domains, finite strains are addressed and elastic nonlinearity is included via a neo-Hookean strain energy potential. The governing equations and boundary conditions are derived; an incremental energy minimization approach is advocated for prediction of equilibrium microstructural morphologies under quasi-static loading protocols. Aspects of the theory are analysed in detail for a material element undergoing simple shear deformation. Exact analytical and/or one-dimensional numerical solutions are obtained in dimensionless form for stress states, stability criteria and order parameter profiles at localized fractures or twinning zones. For sufficient applied strain, the relative likelihood of localized twinning vs. localized fracture is found to depend only on the ratio of twin boundary surface energy to fracture surface energy. Predicted criteria for shear stress-driven fracture or twinning are often found to be in closer agreement with test data for several types of real crystals than those based on the concept of theoretical strength.

15. SUBJECT TERMS
phase field, twinning, fracture, elasticity, crystal, shear deformation

16. SECURITY CLASSIFICATION OF:			17. LIMITATION OF ABSTRACT	18. NUMBER OF PAGES	19a. NAME OF RESPONSIBLE PERSON
					JD Clayton
a. REPORT	b. ABSTRACT	c. THIS PAGE	UU	42	19b. TELEPHONE NUMBER (Include area code)
Unclassified	Unclassified	Unclassified			410-278-6146

Taylor & Francis
Taylor & Francis Group

Nonlinear phase field theory for fracture and twinning with analysis of simple shear

J.D. Clayton[ab*] and J. Knap[a]

[a] *US Army Research Laboratory, Aberdeen Proving Ground, Aberdeen, MD 21005-5066, USA;*
[b] *A. James Clark School of Engineering, University of Maryland, College Park (Adjunct), College Park, MD, USA*

A phase field theory for coupled twinning and fracture in single crystal domains is developed. Distinct order parameters denote twinned and fractured domains, finite strains are addressed and elastic nonlinearity is included via a neo-Hookean strain energy potential. The governing equations and boundary conditions are derived; an incremental energy minimization approach is advocated for prediction of equilibrium microstructural morphologies under quasi-static loading protocols. Aspects of the theory are analysed in detail for a material element undergoing simple shear deformation. Exact analytical and/or one-dimensional numerical solutions are obtained in dimensionless form for stress states, stability criteria and order parameter profiles at localized fractures or twinning zones. For sufficient applied strain, the relative likelihood of localized twinning vs. localized fracture is found to depend only on the ratio of twin boundary surface energy to fracture surface energy. Predicted criteria for shear stress-driven fracture or twinning are often found to be in closer agreement with test data for several types of real crystals than those based on the concept of theoretical strength.

Keywords: phase field; twinning; fracture; elasticity; crystal; shear deformation

1. Introduction

Cleavage fracture and deformation twinning are two fundamental inelastic deformation mechanisms that may occur in crystals when stressed above their elastic limit. Cleavage fracture is defined here as fracture on specific crystallographic planes, typically those of lowest surface energy [1]. Deformation twinning, also known as mechanical twinning, is defined here as twinning induced by mechanical stress [2,3]. Both of these anisotropic mechanisms involve deformation on specific planes (the cleavage plane for fracture or the habit plane for twinning) and tend to be dissipative or thermodynamically irreversible, though reversible or "elastic" twinning is possible in some materials [4]. Local stress concentrations due to fracture (e.g. at crack tips) can induce twinning, and vice versa [2,5–7]. Constitutive models accounting for both phenomena are needed for the prediction of the onset of inelasticity and subsequent mechanical response in materials of interest for engineering applications, including many metals and ceramics.

*Corresponding author. Emails: john.d.clayton1.civ@mail.mil, jdclayt1@umd.edu

Numerous analytical and computational models have been posited to describe fracture or twinning, with resolutions ranging from discrete atoms to macroscopic continua. In the context of continuum mechanical theories, phase field models demonstrate a number of useful characteristics: structural transformations occur naturally via energy minimization [8] or Ginzburg–Landau type kinetics [9], without the need for ad hoc evolution criteria; relatively few material parameters/properties are required; and numerical solutions are regularized (i.e. are rendered mesh-size independent) by a user-defined length parameter associated with interfacial width. Certain regularized variational models incorporating linear elasticity may also demonstrate so-called gamma convergence towards the Griffith theory of fracture as the regularization zone shrinks to a singular surface [10,11]; however, such convergence has apparently not been completely proven for nonlinear elasticity [12]. As detailed in the following paragraphs, phase field theories have already been developed and implemented for independent modelling and simulation of fracture and deformation twinning, but no model seems to have been reported previously that simultaneously addresses both phenomena, in the same analysis, with distinct order parameters for twinned and fractured domains. The development of such a coupled phase field theory is the objective of the present work.

Phase field theories for fracture [13–24], or variational gradient-type theories based on energy minimization similar to phase field approaches [10–12,25], have been under continuous development since the early 2000s. Models have been developed with distinct order parameters for fracture and electric polarization [26–29], and the latter can be physically related to formation of twinned domains in ferroelectrics; this sort of electromechanical twinning differs from deformation twinning associated with partial dislocations considered herein. Though most of the aforementioned fracture theories are posited in the context of small strains, several address finite deformations and nonlinear elasticity [12,15], aspects which are also addressed by the theory developed in the present paper. Also newly addressed in this work is the issue of stability of the nonlinear phase field fracture theory, extending linear elastic analysis of tension considered in prior work [14,30–35] to nonlinear analysis of finite simple shear.

Though not as large as the literature on phase field fracture models, phase field models of deformation twinning have also been documented, with some theories based on geometrically linear elastic response [36–38]. Geometrically nonlinear phase field models of twinning include those of the present authors [5,8,39] applied to a single twin system and [40] applied to martensitic transformations.

Developed in Section 2 of the present paper seems to be the first phase field theory accounting for both fracture and deformation twinning wherein each mechanism is represented by a distinct-order parameter. The model is variational or quasi-static in nature, and is intended for eventual use in finite element simulations that seek equilibrium solutions using incremental energy minimization of a total energy functional that accounts for elastic strain energy and surface energies of cleaved material and twin boundaries. The general theory combines aspects of previous individual nonlinear models for twinning [8,39] and fracture [15]. The minimal necessary material parameters are as follows: the twinning habit plane and twinning eigen-shear, the twin boundary surface energy, the crack plane normal (for anisotropic fracture), the surface energy of fracture and the elastic constants. A numerical parameter is also needed for regularization such that the minimum twin boundary/crack width is finite. Via appropriate choice of energy functional, the model accounts for possible coupling between fracture and twin evolution.

The remaining sections of the paper consider application of various aspects of the general theory of Section 2 towards a one-dimensional simple shear problem. The analysis assumes, a priori, that twinning and/or fracture are confined to occur in the direction of applied shear deformation on a single plane upon which the resolved shear stress is maximum (prior to nucleation) or nearly maximum (after nucleation). Only a single twin system – with its habit plane aligned with the plane of maximum shear stress – and a single mode II crack are considered. From a pragmatic mathematical perspective, these assumptions permit a detailed and thorough analysis of the nonlinear elasticity problem that would not be possible for more complex two- and three-dimensional deformation states involving activity of many twinning systems and/or many cleavage planes. Real crystalline materials tend to have multiple available twinning systems or twin variants [2], but the present restriction to a single system is physically justified for the simple shear problem since deformation twinning is typically driven by resolved shear stress [3,8,41]. For these boundary conditions, the resolved shear stresses on other twin systems in the material would not be sufficiently large for simultaneous nucleation of multiple systems; similarly, twinning in calcite loaded in confined direct shear [42] or indentation [4] demonstrates activity of only a single system associated with maximum shear stress despite the multiplicity of systems available in the crystal. For the above reasons and for conciseness of notation, the theory of Section 2 only accounts for one potential twin system; to address more general problems, extension of the theory to account for multiple twin systems described by distinct-order parameters can be achieved following methods in [8,36–38].

Regarding fracture, most brittle materials tend to fail initially in practice by extensional (mode I) cracking [43], with crack faces oriented for opening along directions of maximum tensile principal stress. For a state of pure shear stress, the maximum tensile stress direction is oriented at an angle of 45° from the shearing direction, i.e. from the direction presumed a priori in the mode II analysis considered later in this work, with the magnitude of the maximum tensile stress equal (or nearly so) to the applied/resolved shear stress. However, the shearing mode of fracture would be preferred in a material with a lower fracture strength for tangential/sliding modes than for tensile modes, or for a highly anisotropic (e.g. mica-like) solid oriented with cleavage planes parallel to the shearing direction. Furthermore, the study of pure shearing-type fracture is of theoretical interest because results can be compared with other models of "theoretical shear strength" as originated by Frenkel [44] and used to provide fundamental insight into aspects of atomic bonding [45] and upper bounds for stresses leading to homogeneous dislocation nucleation and glide [46]. Values of theoretical shear strength obtained under conditions of pure or simple shear loading can be used in failure criteria for brittle materials undergoing other loading protocols in which all three principal stresses are compressive, wherein a maximum tensile stress criterion would be ineffective. For example, theoretical shear strength arguments have been used to describe the onset of fracture in shock compression [47,48] (and see later Section 4 of this work), and shear fracture strength is of high importance for indentation and ballistic loading [49] in regions of material far from free surfaces where tensile cracking may occur, as well as in special direct shear experiments [42] where confinement precludes opening of mode I cracks. The analytical solutions derived later do not explicitly account for large compressive hydrostatic pressures that accompany planar shock compression, for example, but theoretical shear strengths derived from a tractable analysis of the simple shear problem may be transferable, as has been assumed elsewhere [47,50], to the former type of (shock) loading that cannot be subjected to a complete analytical treatment using the phase field

approach. Finally, analytical solutions to the simple shear problem with a single pure mode II crack enable isolation of deviatoric features of the model that can be used for validation of numerical methods (e.g. finite element solutions to be obtained in future work) and comparison with sharp interface (e.g. Griffith-type, see Section 4 representations; similar studies have been undertaken for shear in a geometrically linear setting [25].

Interactions between fractured and transformed/twinned zones have been reported for crystalline solids undergoing simultaneous fracture and twinning or phase transformations, and such interactions have been modelled elsewhere via phase field numerical simulations of ferroelectrics [29] and austenitic–martensitic steels [51]. Complex stress states may emerge as a result, and transformation kinetics influence crack paths and vice versa. The present complete theory, if implemented numerically for two- or three-dimensional simulations, would allow for prediction of incremental equilibrium states corresponding to such phenomena, including crack branching affected by twinning under quasi-static loading, for example. However, the particular analytical solutions derived for simple shear with cracks and twins aligned parallel to a single direction do not permit consideration of such complex stress states and changes in crack paths.

The governing equations and nondimensional forms are derived for the simple shear problem admitting both fracture and twinning in Section 3.1. The possibility of damage and twinning to appear sequentially or simultaneously and the relative likelihood of complete mode II fracture vs. localized twinning are addressed in Section 3.2. Section 3.3 considers mode II fracture in the absence of twinning: nondimensional analytical solutions for homogeneous damage, stability criteria and localized complete fracture, as well as numerical solutions for inhomogeneous damage. Twinning under simple shear in the absence of damage is then considered in Section 3.4 as another particular case: nondimensional analytical solutions for homogeneous elasticity, stability and numerical solutions for localized complete twinning. Predicted critical stresses associated with shear fracture or twin nucleation are compared with other models and data from the literature for several real crystalline materials in Section 4. Conclusions follow in Section 5.

Notation of modern continuum mechanics/physics is used. Vectors and tensors are written in bold font and are referred to a Cartesian coordinate system. Superscripts T, -1 and $-T$ denote the transpose, inverse and inverse-transpose. In indicial notation with summation over repeated indices, the dot product, double-dot product and outer product obey $\boldsymbol{a} \cdot \boldsymbol{b} = a_K b_K$, $\boldsymbol{A} : \boldsymbol{B} = A_{IJ} B_{IJ}$, and $(\boldsymbol{a} \otimes \boldsymbol{b})_{IJ} = a_I b_J$.

2. Nonlinear phase field theory

The present theory essentially combines previous phase field approaches for twinning [8,39] and fracture [15] in a way general enough to permit physically realistic coupling of the two phenomena. A geometrically nonlinear theory is considered, accounting for finite strains, finite rotations and nonlinear elastic response.

2.1. *Order parameters and kinematics*

Let X denote material coordinates and t time. Let $\eta(X, t)$ denote the order parameter associated with twinning on a single twin system (see e.g. [8] for extension to multiple twin systems):

$$\eta(X, t) = 0 \forall X \in \text{parent},$$
$$\eta(X, t) = 1 \forall X \in \text{twin},$$
$$\eta(X, t) \in (0, 1) \forall X \in \text{twin boundary}. \tag{2.1}$$

Let $\xi(X, t)$ denote the order parameter associated with fracture (possibly, but not necessarily, concentrated on a single cleavage plane):

$$\xi(X, t) = 0 \forall X \in \text{intact solid},$$
$$\xi(X, t) = 1 \forall X \in \text{failed domain},$$
$$\xi(X, t) \in (0, 1) \forall X \in \text{cohesive boundary}. \tag{2.2}$$

Motion is $x(X, t) = X + u(X, t)$ with u the displacement. The deformation gradient is the two-point tensor

$$F = \nabla x = 1 + \nabla u, \tag{2.3}$$

where $\nabla_K(\cdot) = \partial(\cdot)/\partial X_K$ is the material gradient. The deformation gradient is split multiplicatively as [8]

$$F = F^E F^\eta. \tag{2.4}$$

Twinning deformation is the simple shear

$$F^\eta(\eta) = 1 + [\varphi(\eta)\gamma_0]s \otimes m, \quad \det F^\eta = 1 + \varphi\gamma_0 s \cdot m = 1. \tag{2.5}$$

Orthogonal unit vectors (in material coordinates) in the twinning direction and normal to twinning plane are s and m, the magnitude of maximum twinning shear is γ_0, and $\varphi : [0, 1] \to [0, 1]$ is a continuous and monotonically increasing interpolation function satisfying $\varphi(0) = 0$ and $\varphi(1) = 1$. Define the symmetric elastic material deformation tensor and the Jacobian determinant:

$$C = F^{E\,T}F^E, \quad J = \det F^E = \det F = \sqrt{\det C}. \tag{2.6}$$

An incremental or quasi-static theory is the focus, with explicit dependence of field variables on t omitted.

A few remarks regarding compatibility are in order. Neither F^E nor F^η is generally integrable to a vector field; i.e. elastic and twin deformation mappings in that case are generally anholonomic [52,53], meaning

$$\nabla \times F^\eta \neq 0, \quad \bar{\nabla} \times F^{E\,-1} \neq 0, \tag{2.7}$$

where $\bar{\nabla}$ is the gradient with respect to spatial coordinates [i.e. $\bar{\nabla}_k(\cdot) = \partial(\cdot)/\partial x_k = \nabla_J(\cdot)F_{Jk}^{-1}$]. Total deformation gradient F and its inverse are compatible by definition:

$$\nabla \times F = \nabla \times \nabla x = 0, \quad \bar{\nabla} \times F^{-1} = \bar{\nabla} \times \bar{\nabla}X = 0. \tag{2.8}$$

In contrast to fracture mechanics models wherein discrete cracks are resolved explicitly in terms of jump discontinuities in displacement (leading to singularities in F), in the phase field approach the displacement field $u(X)$ is continuous and continuously differentiable. As explained later in Section 2.3, failure is captured via a reduction in local elastic stiffness (i.e. an increase in compliance) at a given material point X, similar to continuum damage mechanics theories. Accordingly, an advantage of the phase field method over computational models involving discontinuous fields (e.g. cohesive finite elements) is that conventional

finite element or finite difference schemes can be invoked in the former, requiring no special treatment or tracking of surfaces of discontinuity. The present phase field theory also differs from other finite strain continuum damage mechanics models wherein incompatible components of the deformation gradient are used to represent irreversible deformation associated with local fractures within a volume element of material [54–56].

2.2. *Governing equations*

The total energy functional for an initially homogeneous body Ω with uniform material properties is

$$\Psi(\boldsymbol{x}, \eta, \xi) = \int_{\Omega} [W(\nabla \boldsymbol{x}, \eta, \xi) + f(\eta, \xi, \nabla\eta, \nabla\xi)] \mathrm{d}V. \tag{2.9}$$

In the reference configuration, the body occupies volume V and is enclosed by surface S with unit outward normal $\boldsymbol{n}$. In the nonlinear theory, strain energy per unit reference configuration volume W is of the form

$$W = W[\boldsymbol{C}(\boldsymbol{F}, \eta), \eta, \xi]. \tag{2.10}$$

Stationary points of the total energy functional Ψ are obtained as solutions of

$$\delta\Psi = \oint_{\partial\Omega} (\boldsymbol{t} \cdot \delta\boldsymbol{x} + r\delta\eta + s\delta\xi) \mathrm{d}S, \tag{2.11}$$

where, from (2.9),

$$\delta\Psi = \int_{\Omega} \left[\frac{\partial W}{\partial \boldsymbol{F}} : \nabla\delta\boldsymbol{x} + \frac{\partial W}{\partial \eta}\delta\eta + \frac{\partial W}{\partial \xi}\delta\xi + \frac{\partial f}{\partial \eta}\delta\eta + \frac{\partial f}{\partial \xi}\delta\xi + \frac{\partial f}{\partial \nabla\eta} \cdot \nabla\delta\eta + \frac{\partial f}{\partial \nabla\xi} \cdot \nabla\delta\xi \right] \mathrm{d}V. \tag{2.12}$$

Assuming fields are sufficiently smooth, the following general local equilibrium equations (i.e. Euler–Lagrange equations) and boundary conditions are then derived by extending, for example, the procedure involving the divergence theorem and integration by parts detailed in [8]:

$$\nabla \cdot \frac{\partial W}{\partial \boldsymbol{F}}\Big|_{\eta, \xi} = \nabla \cdot \boldsymbol{P} = \boldsymbol{0}, \quad \boldsymbol{P} = \frac{\partial W}{\partial \boldsymbol{F}}\Big|_{\eta, \xi}; \tag{2.13}$$

$$\frac{\partial f}{\partial \eta} - \nabla \cdot \frac{\partial f}{\partial \nabla\eta} + \frac{\partial W}{\partial \eta}\Big|_{\boldsymbol{F}, \xi} = 0, \quad \frac{\partial f}{\partial \xi} - \nabla \cdot \frac{\partial f}{\partial \nabla\xi} + \frac{\partial W}{\partial \xi}\Big|_{\boldsymbol{F}, \eta} = 0; \tag{2.14}$$

$$\boldsymbol{t} = \boldsymbol{P} \cdot \boldsymbol{n}, \quad r = \frac{\partial f}{\partial \nabla\eta} \cdot \boldsymbol{n}, \quad s = \frac{\partial f}{\partial \nabla\xi} \cdot \boldsymbol{n}. \tag{2.15}$$

The traction per unit reference area is $\boldsymbol{t}$; the conjugate force to order parameter η is r; the conjugate force to order parameter ξ is s. These equations apply for the general framework of (2.9), with (2.13) and (2.14) holding within domain Ω and (2.15) holding on its external boundary $\partial\Omega$.

The interfacial energy per unit reference volume considered here is of the general form

$$f(\eta, \xi, \nabla\eta, \nabla\xi) = f_0(\eta, \xi) + g_0(\xi) + f_1(\eta, \xi, \nabla\eta) + g_1(\eta, \xi, \nabla\xi). \tag{2.16}$$

Taking this into account, equilibrium Equation (2.14) and boundary conditions (2.15) can be expressed as

$$\frac{\partial f_0}{\partial \eta} + \frac{\partial f_1}{\partial \eta} + \frac{\partial g_1}{\partial \eta} - \nabla \cdot \frac{\partial f_1}{\partial \nabla \eta} + \frac{\partial W}{\partial \eta}\Big|_{F,\xi} = 0; \qquad (2.17)$$

$$\frac{\partial f_0}{\partial \xi} + \frac{\partial g_0}{\partial \xi} + \frac{\partial f_1}{\partial \xi} + \frac{\partial g_1}{\partial \xi} - \nabla \cdot \frac{\partial g_1}{\partial \nabla \xi} + \frac{\partial W}{\partial \xi}\Big|_{F,\eta} = 0; \qquad (2.18)$$

$$\boldsymbol{t} = \boldsymbol{P} \cdot \boldsymbol{n}, \quad r = \frac{\partial f_1}{\partial \nabla \eta} \cdot \boldsymbol{n}, \quad s = \frac{\partial g_1}{\partial \nabla \xi} \cdot \boldsymbol{n}. \qquad (2.19)$$

2.3. *Compressible neo-Hookean elasticity*

Similar to previous phase field models for twinning [5,39], compressible neo-Hookean elasticity is now considered, where for modelling elasticity and fracture,

$$W = \tfrac{1}{2}[\lambda(\ln J)^2 - \mu(2\ln J - \mathrm{tr}\boldsymbol{C} + 3)]. \qquad (2.20)$$

Lamé coefficients μ and λ depend on ξ and possibly J:

$$\mu(\xi) = \mu_0\{\zeta + (1-\zeta)[1-\phi(\xi)]\}, \quad \lambda = k(\xi, J) - \tfrac{2}{3}\mu(\xi). \qquad (2.21)$$

Here, $\phi : [0,1] \to [0,1]$ is a continuous monotonic interpolation function satisfying $\phi(0) = 0$ and $\phi(1) = 1$, and ζ is a small scalar constant subject to $0 < \zeta \ll 1$. A particular example function is

$$\phi(\xi) = 1 - (1-\xi)^2. \qquad (2.22)$$

The shear modulus μ degrades from its reference value μ_0 to a minimum value $\zeta\mu_0$ in fully fractured domains. The constant ζ ensures that the material maintains a minimal residual stiffness when fully fractured [22,26]; for solution of some (but not all) boundary value problems, it may be needed for numerical stability and is not considered a material property. For conciseness, a degradation function $\hat{\phi}$ is introduced:

$$\hat{\phi}(\xi) = \zeta + (1-\zeta)[1-\phi(\xi)] \Rightarrow \mu = \mu_0\hat{\phi}. \qquad (2.23)$$

Note that the prescription of a regularized variational formulation of fracture in [10] is recovered when the residual stiffness is omitted:

$$\zeta = 0 \Rightarrow \hat{\phi}(\xi) = (1-\xi)^2 \Rightarrow \mu(\xi) = [1-\phi(\xi)]\mu_0 = (1-\xi)^2\mu_0. \qquad (2.24)$$

A quadratic degradation of elastic stiffness with damage has likewise been used in a number of other phase field and variational models of fracture [11,14,20,22]. The bulk modulus k degrades in tension but not in compression, in order to prohibit interpenetration [25]:

$$k = \left(\lambda_0 + \tfrac{2}{3}\mu_0\right)[\langle J - 1\rangle\hat{\phi}(\xi) + \langle 1 - J\rangle^*], \qquad (2.25)$$

where λ_0 is the constant initial Lamé modulus and $\langle x \rangle = 1 \forall x > 0$, $\langle x \rangle = 0 \forall x \leq 0$, $\langle x \rangle^* = 1 \forall x \geq 0$, and $\langle x \rangle^* = 0 \forall x < 0$. The above neo-Hookean model is restricted to isotropic elasticity, a notable approximation for real crystals. For anisotropic elastic constants, the model must be extended to account for transformation (reflection or rotation) of the reference frame of the crystal lattice commensurate with twinning, as has been

elaborated for a nonlinear model based on the Green strain [8]. However, since Green strain-type theories incorporating higher order elastic constants tend towards instability under large compression [57,58], formulation of a nonlinear anisotropic theory incorporating another strain tensor such as the material Eulerian strain [59,60] or material logarithmic strain [61] may be prudent in the future.

Further justification of the use of a nonlinear elastic model, and compressible neo-Hookean elasticity in particular, is now discussed. In brittle solids undergoing fracture (but not twinning), linear elasticity may be sufficient if failure occurs before large deformations are attained; recent phase field simulations [15] have demonstrated very similar results for crack nucleation in linear and nonlinear elastic brittle solids. However, the present work is concerned with both fracture and deformation twinning, and accurate depiction of the latter usually requires a finite deformation description [62]. Twinning shear deformation γ_0 is often large, for example a value of $\frac{\sqrt{2}}{2}$ for the most common mode in cubic crystals [2]. Previous phase field simulations [5,39] have demonstrated differences in predictions for twin nucleation and growth among linear elastic and neo-Hookean models. The neo-Hookean model used herein has also been shown to provide a reasonable two-parameter depiction of the increasing bulk stiffness of some crystalline solids (calcite and sapphire) under finite volumetric compression, in contrast to linear elasticity wherein the bulk modulus is constant. Neo-Hookean elasticity has also been incorporated elsewhere in a nonlinear phase field model of twinning in crystalline CuAlNi (martensitic phase) [40]. The distinction between the compressible neo-Hookean potential used here and incompressible neo-Hookean elasticity often used for polymers such as plastics and rubber-type materials is also noted. In ductile crystalline solids, crack tip plasticity often ensues prior to attainment of large elastic deformations, rendering consideration of dislocation motion more important than nonlinear elastic effects. As remarked later in Section 4, extensions of the current model framework would be necessary for modelling dislocation plasticity distinct from twinning.

For twinning on a single plane, with a double-well potential and isotropic surface energy,

$$f_0(\eta, \xi) = A\eta^2(1 - \eta)^2 \hat{\iota}(\xi), \tag{2.26}$$

$$f_1(\xi, \nabla\eta) = \boldsymbol{\kappa}(\xi) : (\nabla\eta \otimes \nabla\eta), \quad \boldsymbol{\kappa}(\xi) = \kappa_0 \hat{\iota}(\xi)\mathbf{1}, \tag{2.27}$$

where the constants A and κ_0 are related to the twin boundary surface energy Γ and the thickness l as [8]

$$A = 12\Gamma/l, \quad \kappa_0 = \tfrac{3}{4}\Gamma l. \tag{2.28}$$

Note that f_0 and $\boldsymbol{\kappa}$ can degrade with ξ via function $\hat{\iota}$; this can prevent a twin boundary that crosses a free surface from having duplicate surface energy, for example. The degradation function $\hat{\iota} : [0, 1] \rightarrow [0, 1]$ obeys

$$\hat{\iota}(0) = 1, \quad \hat{\iota}' = \mathrm{d}\hat{\iota}/\mathrm{d}\xi. \tag{2.29}$$

A candidate choice is $\hat{\iota} = \hat{\phi}$, meaning twin boundary energy and elastic shear modulus degrade analogously.

For cleavage fracture on a preferred plane, it is assumed that the orientation of such a plane is known a priori. For example, this would be a plane or family planes of low surface energy or low intrinsic strength in a crystal. Considered herein is a single plane. A unit vector (in material coordinates) normal to this cleavage plane is M. Let B, ω_0 and β denote material constants. For the present fracture model,

$$g_0(\xi) = B\xi^2, \tag{2.30}$$

$$g_1(\nabla\xi) = \boldsymbol{\omega} : (\nabla\xi \otimes \nabla\xi), \quad \boldsymbol{\omega} = \omega_0[\mathbf{1} + \beta(\mathbf{1} - \boldsymbol{M} \otimes \boldsymbol{M})]. \tag{2.31}$$

The crack thickness h and fracture surface energy Υ are related as [22]

$$B = \Upsilon/h, \quad \omega_0 = \Upsilon h. \tag{2.32}$$

Setting $\beta \gg 1$ greatly increases the surface energy of fracture on planes not normal to $\boldsymbol{M}$; β is thus a penalty factor, not a typical material property. Setting $\beta = 0$ results in isotropic damage. This isotropic continuum representation, with $g_0 \propto \xi^2$, has been shown to converge to the correct surface energy of a singular surface as $l \to 0$ [10,11] and has been used in a number of recent continuum models [12,14,20,22,25].

Consider now the specific constitutive model of (2.20)–(2.32) incorporating compressible neo-Hookean elasticity, a double-well potential for twinning with eigen-strain interpolator $\varphi(\eta)$ and a quadratic potential for fracture with degradation function $\hat{\phi}(\xi)$. Euler–Lagrange equations for order parameters (2.17) and (2.18) become, with τ and σ interpreted as elastic driving forces associated with twinning and fracture,

$$\tau = \frac{\partial W}{\partial \eta}\bigg|_{\boldsymbol{F},\xi} = 2\kappa_0\{\hat{\iota}(\xi)\nabla^2\eta + \hat{\iota}'(\xi)\nabla\xi \cdot \nabla\eta\} - 2A\eta(1 - 3\eta + 2\eta^2)\hat{\iota}(\xi); \tag{2.33}$$

$$\varsigma = \frac{\partial W}{\partial \xi}\bigg|_{\boldsymbol{F},\eta} = 2\omega_0[\nabla^2\xi + \beta(\nabla^2\xi - \boldsymbol{M} \otimes \boldsymbol{M} : \nabla\nabla\,\xi)]$$
$$- 2B\xi - [\kappa_0|\nabla\eta|^2 + A\eta^2(1 - \eta)^2]\hat{\iota}'(\xi). \tag{2.34}$$

Primes denote derivatives of functions of one variable, e.g. $\varphi' = \mathrm{d}\varphi/\mathrm{d}\eta$ and $\varphi'' = \mathrm{d}^2\varphi/\mathrm{d}\eta^2$. For simple problems (e.g. one-dimensional problems such as those considered later in Section 3), it may be possible to find solutions of (2.13) and (2.33)–(2.34) directly and analytically. General two- and three-dimensional boundary value problems will require numerical solutions, which can be found incrementally using the finite element method [8] wherein boundary conditions for displacement and order parameters (or their conjugate forces) are updated during each load increment. For certain boundary conditions, candidate solutions [i.e. fields $\boldsymbol{x}(\boldsymbol{X}), \eta(\boldsymbol{X}), \xi(\boldsymbol{X})$] are obtained that minimize $\Psi(\boldsymbol{x}, \eta, \xi)$ and thus satisfy (2.11). However, because Ψ is generally nonconvex, multiple (local) minima may exist, and therefore solutions may be nonunique; when Ψ of such a local minima exceeds the global minimum energy, then such a solution is said to be metastable. To ensure irreversibility of crack extension, constraints such as $\delta\xi(\boldsymbol{X}) \geq 0$ for $\xi(\boldsymbol{X})$ exceeding some threshold value can be imposed [12,15].

A number of different interpolation functions φ have been used for interpolation of twinning shear [5,8,9,40]. A particular function considered later is

$$\varphi(\eta) = \eta^2(3 - 2\eta), \tag{2.35}$$

with derivatives

$$\varphi'(\eta) = 6\eta(1 - \eta), \quad \varphi''(\eta) = 6(1 - 2\eta), \tag{2.36}$$

and useful properties

$$\varphi(0) = 0, \quad \varphi(1) = 1, \quad \varphi\left(\tfrac{1}{2}\right) = \tfrac{1}{2}; \quad \varphi'(0) = \varphi'(1) = 0; \quad \varphi''\left(\tfrac{1}{2}\right) = 0. \tag{2.37}$$

For completeness, derivatives and special values of function $\hat{\phi}(\xi)$ of (2.23) with ϕ of (2.22) are listed:

$$\hat{\phi}'(\xi) = -2(1-\zeta)(1-\xi), \quad \hat{\phi}''(\xi) = 2(1-\zeta); \tag{2.38}$$

$$\hat{\phi}(0) = 1, \quad \hat{\phi}(1) = \zeta; \quad \hat{\phi}'(0) = -2(1-\zeta), \quad \hat{\phi}'(1) = 0. \tag{2.39}$$

Further remarks on a number of scalar functions entering the total energy functional are now given, specifically f_0, f_1, g_0, g_1, ϕ, $\hat{\phi}$, $\hat{\iota}$ and φ. None of these functions is determined uniquely by mathematical or physical criteria, though relatively simple forms for all are chosen that satisfy stated necessary conditions associated with endpoint values, continuity and smoothness, and possible symmetry. In particular, f_0 includes a double-well potential typically used in phase field theory [8,39], though other higher order polynomial forms have been prescribed elsewhere for twinning energetics [36,38]. Quadratic forms prescribed for gradient terms f_1 and g_1 are standard in phase field models. Quadratic term g_0 is used in conjunction with degradation function ϕ because, for linear elasticity in the absence of twinning, these provide gamma convergence of the regularized fracture energy to the surface energy in discrete (Griffith-type) fracture mechanics [10,11]. The model used here for stiffness degradation in tension and shear, incorporating $\hat{\phi}$ with residual strength ζ, agrees with representations used elsewhere [12,15]; however, it has been verified in variational simulations of fracture [25] that quantitative predictions depend on choice of ζ, and thus implicitly on choice of $\hat{\phi}$. Coupling function $\hat{\iota}$ is new to the present theory (since no other coupled fracture-twinning phase field theory is known to the authors) and its choice does influence the availability of analytical solutions, as discussed in Section 3.2. Interpolation function φ has been used in other finite strain models involving twinning [5,8,39] and phase transformations [9]; prior work has verified that use of a different interpolation function (specifically an exponential function of Fermi-Dirac type) can affect quantitative predictions for twin nucleation [5]. As shown later in Section 3.4.3, stability is affected by the derivative of φ at $\eta = 0$.

The present variational framework for twinning and fracture does not account for effects of loading rate, temperature or explicit dissipation. Mathematically, it is sufficient to state that the theory is limited to isothermal equilibrium solutions; physically, this corresponds to neglect of local dynamics that presumably occur on very short time scales for problems of interest. Transients, rate effects and path dependence of solutions could be included by replacing the equilibrium equations for order parameters by corresponding kinetic equations dictating their evolution. For example, a standard approach [9,18,20,40,63,64] involves replacing (2.17) and (2.18) with Ginzburg–Landau type gradient flow equations

$$\dot{\eta} = -M_\eta \frac{\delta\psi}{\delta\eta} = -M_\eta \left(\frac{\partial\psi}{\partial\eta} - \nabla \cdot \frac{\partial\psi}{\partial\nabla\eta} \right), \quad \dot{\xi} = -M_\xi \frac{\delta\psi}{\delta\xi} = -M_\xi \left(\frac{\partial\psi}{\partial\xi} - \nabla \cdot \frac{\partial\psi}{\partial\nabla\xi} \right). \tag{2.40}$$

Here, the superposed dot denotes a material time derivative (X fixed), M_η and M_ξ are positive mobility coefficients (inverse viscosities), and $\psi = W + f$ is total free energy per unit reference volume. These equations can be easily generalized to account for kinetic coupling via replacement of scalar mobilities with a symmetric 2×2 tensor [8,9]. For isothermal problems, thermal effects can be included via allowance of mobilities, as well as surface energies and elastic coefficients, to depend on temperature T. For problems wherein temperature changes occur, the free energy function must be extended to include explicit dependence on temperature change (i.e. specific heat and thermoelastic coupling), and an

energy balance must be introduced relating changes in temperature, dissipated energy from inelastic work and viscosity, and possible heat conduction [65]. The present assumption of static mechanical equilibrium is also strong and would be inappropriate for problems of crack nucleation and extension driven by elastic waves, for example, dynamic impact involving spall. When inertial effects are important, the balance of linear momentum (2.13) must be extended to include material acceleration as in [14,66].

3. Analysis of simple shear

Considered in Section 3 is application of the general theory of Section 2 towards a problem of simple shear deformation. Governing equations of Section 2 are specialized towards this deformation state in Section 3.1. The general case wherein fracture and deformation twinning may occur, either sequentially or simultaneously, in an element of material subjected to simple shear loading is studied in Section 3.2, along with the degenerate case of homogeneous purely elastic deformation. Considered in Section 3.3 is a reduction of the general treatment of Section 3.2 to the case where fracture/damage may occur but twinning is prohibited. Considered in Section 3.4 is a reduction of the treatment of Section 3.2 to the case where twinning may occur but fracture is prohibited. Solutions are addressed for the six scenarios shown in Figure 1; notation is described in detail below.

3.1. *Governing equations*

Consider a domain Ω of initially homogeneous material in the $X_1 - X_2$ plane. By construction, during a deformation-fracture-twinning process, assume that fields $\boldsymbol{u}$, ξ, and η depend only on the X_1 coordinate and that displacement is further restricted to only occur in the X_2 direction, i.e. $\boldsymbol{u}(X_1) = v(X)\boldsymbol{e}_2$, where $(X_1, X_2, X_3) = (X, Y, Z)$ and $\boldsymbol{e}_2$ is a unit vector tangent to Y. The length of the body in the X direction is L, such that $X \in [0, L]$. The width in the Y direction does not explicitly enter the problem, but the body is considered "wide" enough to eliminate boundary effects that may lead to dependence of the solution on Y.

The order parameters for fracture, twinning and their spatial gradients become the scalar fields

$$\xi = \xi(X), \quad \nabla\xi = \partial\xi/\partial X = \xi'(X), \quad \nabla\nabla\xi = \nabla^2\xi = \partial^2\xi/\partial X^2 = \xi''(X); \quad (3.1)$$

$$\eta = \eta(X), \quad \nabla\eta = \partial\eta/\partial X = \eta'(X), \quad \nabla\nabla\eta = \nabla^2\eta = \partial^2\eta/\partial X^2 = \eta''(X). \quad (3.2)$$

The simple shear deformation and the deformation gradient are, respectively,

$$x = X, \qquad y = Y + v(X), \qquad z = Z; \quad (3.3)$$

$$\boldsymbol{F} = \boldsymbol{1} + \gamma\,\boldsymbol{e}_2 \otimes \boldsymbol{e}_1; \qquad \gamma(X) = \partial v/\partial X = v', \qquad J = \det \boldsymbol{F} = 1. \quad (3.4)$$

Twinning is restricted to occur in the Y direction with habit plane(s) normal to X, giving

$$[\boldsymbol{F}^\eta(\eta)] = \begin{bmatrix} 1 & 0 & 0 \\ \gamma_0\varphi(\eta) & 1 & 0 \\ 0 & 0 & 1 \end{bmatrix}, \qquad [\boldsymbol{s}] = \begin{bmatrix} 0 \\ 1 \\ 0 \end{bmatrix}, \qquad [\boldsymbol{m}] = \begin{bmatrix} 1 \\ 0 \\ 0 \end{bmatrix}. \quad (3.5)$$
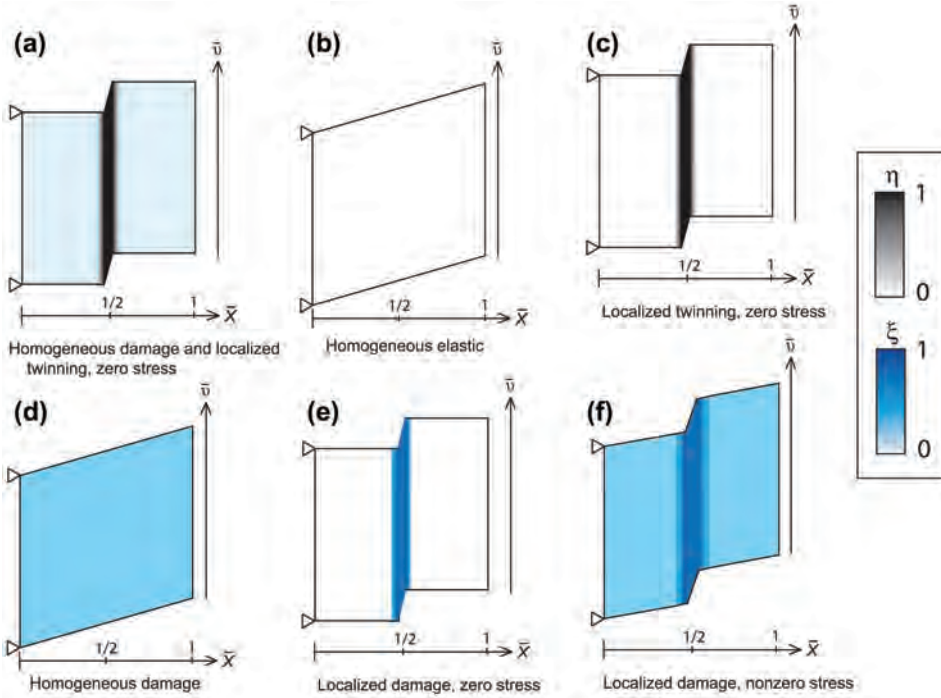
Figure 1. (colour online) Simple shearing problem: (a) coupled twinning and fracture, (b) no twinning or fracture, (c) stress-free twinning, (d) homogeneous damage, (e) localized complete fracture and (f) inhomogeneous damage. Order parameters for twinning and fracture are η and ξ; applied dimensionless shear displacement is $\bar{\upsilon}$.

The elastic deformation gradient, elastic volume change, elastic deformation tensor and its trace are

$$[\boldsymbol{F}^{\mathrm{E}}(\gamma, \eta)] = [\boldsymbol{F}][\boldsymbol{F}^{\eta-1}] = \begin{bmatrix} 1 & 0 & 0 \\ \gamma - \gamma_0 \varphi(\eta) & 1 & 0 \\ 0 & 0 & 1 \end{bmatrix}, \qquad \det \boldsymbol{F}^{\mathrm{E}} = J/J^{\eta} = 1; \qquad (3.6)$$

$$[\boldsymbol{C}] = \begin{bmatrix} 1 + (\gamma - \gamma_0 \varphi)^2 & \gamma - \gamma_0 \varphi & 0 \\ \gamma - \gamma_0 \varphi & 1 & 0 \\ 0 & 0 & 1 \end{bmatrix}, \qquad \mathrm{tr}\boldsymbol{C} = 3 + (\gamma - \gamma_0 \varphi)^2. \qquad (3.7)$$

Assume $\zeta = 0$ such that shear modulus degradation function $\hat{\phi}(\xi) = (1 - \xi)^2$. The twin boundary energy degradation function $\hat{\iota}$ obeys (2.29) but is otherwise left unspecified at present. Strain energy density of (2.20) becomes, for the present simple shear geometry with $\varphi = \varphi(\eta)$,

$$W[\gamma(X), \xi(X), \eta(X)] = \tfrac{1}{2}\mu(\mathrm{tr}\boldsymbol{C} - 3) = \tfrac{1}{2}\mu_0(1 - \xi)^2(\gamma - \gamma_0\varphi)^2. \qquad (3.8)$$

It is assumed for simplicity that the regularization length parameter $h = l$ is the same for twin boundary thickness or fracture interfacial thickness. Then (2.30)–(2.32) become

$$g_0[\xi(X)] = \Upsilon\xi^2/l, \qquad \boldsymbol{\omega} : \nabla\xi \otimes \nabla\xi = \Upsilon l[\xi'(X)]^2. \qquad (3.9)$$

A reduction of the fully three-dimensional theory of Section 2.3 to the one-dimensional scenario considered here can be achieved by setting $\beta \to \infty$ in (2.31) with $\boldsymbol{M} = \boldsymbol{e}_1$, such that fracture energy contribution $g_1(\nabla \xi) \to \infty$ for cracks of orientations differ from those parallel to the Y axis. Thus, potential crack geometries are restricted to those shown in Figure 1 since cracks of other orientations would tend towards infinite energy. Aspects of the twinning model in (2.26)–(2.28) reduce to

$$f_0[\eta(X), \xi(X)] = (12\Gamma/l)\eta^2(1-\eta)^2\hat{\imath}, \qquad \boldsymbol{\kappa} : \nabla\eta \otimes \nabla\eta = (3\Gamma l/4)[\eta'(X)]^2\hat{\imath}. \quad (3.10)$$

The total energy functional (2.9) becomes, per unit cross-sectional area,

$$\begin{aligned}
\Psi &= \int_0^L (W + f_0 + g_0 + \boldsymbol{\kappa} : \nabla\eta \otimes \nabla\eta + \boldsymbol{\omega} : \nabla\xi \otimes \nabla\xi)\mathrm{d}X \\
&= \int_0^L \left\{ \tfrac{1}{2}\mu_0(1-\xi)^2(\gamma - \gamma_0\varphi)^2 + (12\Gamma/l)\hat{\imath}\eta^2(1-\eta)^2 + \Upsilon\xi^2/l + \tfrac{3}{4}\Gamma l\hat{\imath}[\eta'(X)]^2 \right. \\
&\qquad\quad \left. + \Upsilon l[\xi'(X)]^2 \right\}\mathrm{d}X.
\end{aligned} \quad (3.11)$$

From (2.13) and (2.20) with $J = 1$, the stress tensor is $\boldsymbol{P} = \mu(\boldsymbol{F}^{\mathrm{E}} - \boldsymbol{F}^{\mathrm{E-T}})\boldsymbol{F}^{\eta-\mathrm{T}}$. It follows that the only nonzero components of the first Piola–Kirchhoff stress are

$$P(X) = P_{xY} = P_{yX} = \mu_0(1-\xi)^2(\gamma - \gamma_0\varphi), \qquad P_{yY}(X) = -\mu_0(1-\xi)^2(\gamma - \gamma_0\varphi)\gamma_0\varphi. \quad (3.12)$$

The equation for stress equilibrium in (2.13) ($\nabla \cdot \boldsymbol{P} = \boldsymbol{0}$) results in the single nontrivial equation

$$P'(X) = \partial P/\partial X = 0 \Rightarrow P = \text{constant}. \quad (3.13)$$

The conjugate driving force for fracture introduced in the first of (2.34) is

$$\varsigma(X) = \partial W/\partial\xi = -\mu_0(1-\xi)(\gamma - \gamma_0\varphi)^2. \quad (3.14)$$

The Euler–Lagrange equation for fracture order parameter equilibrium, also in (2.34), reduces to

$$\mu_0(1-\xi)(\gamma - \gamma_0\varphi)^2 - 2\Upsilon\xi/l + 2\Upsilon l\xi'' - \hat{\imath}'[3\Gamma l(\eta')^2/4 + 12\Gamma\eta^2(1-\eta)^2/l] = 0. \quad (3.15)$$

The conjugate driving force for twinning introduced in the first of (2.33) is

$$\tau(X) = \partial W/\partial\eta = -\mu_0\gamma_0(1-\xi)^2(\gamma - \gamma_0\varphi)\varphi', \quad (3.16)$$

where $\varphi' = \mathrm{d}\varphi/\mathrm{d}\eta$. Twinning order parameter equilibrium, i.e. the second of (2.33), requires

$$\mu_0\gamma_0(1-\xi)^2(\gamma - \gamma_0\varphi)\varphi' + \tfrac{3}{2}\Gamma l[\hat{\imath}\eta'' + \hat{\imath}'\eta'\xi'] - 24\Gamma\hat{\imath}\eta(1 - 3\eta + 2\eta^2)/l = 0. \quad (3.17)$$

Finding simultaneous solutions to (3.13), (3.15), and (3.17), given yet to be prescribed boundary conditions, becomes more straightforward upon transformation of variables to normalized dimensionless form. Denoting transformed variables by an overbar, define

$$\bar{X} = X/L, \qquad \bar{l} = l/L, \qquad \bar{v} = v\sqrt{\mu_0/(\Upsilon L)}, \qquad \bar{\mu}_0 = 1, \qquad \bar{\Psi} = \Psi L/(2\Upsilon). \tag{3.18}$$

These definitions result in

$$\bar{\gamma} = \partial\bar{v}/\partial\bar{X} = \gamma\sqrt{\mu_0 L/\Upsilon}, \quad \bar{\gamma}_0 = \gamma_0\sqrt{\mu_0 L/\Upsilon}, \quad \bar{P} = P\sqrt{L/(\mu_0\Upsilon)}; \tag{3.19}$$

$$\bar{\xi}' = \partial\xi/\partial\bar{X} = \xi' L, \qquad \bar{\xi}'' = \partial^2\xi/\partial\bar{X}^2 = \xi'' L^2; \tag{3.20}$$

$$\bar{\eta}' = \partial\eta/\partial\bar{X} = \eta' L, \qquad \bar{\eta}'' = \partial^2\eta/\partial\bar{X}^2 = \eta'' L^2. \tag{3.21}$$

The order parameters $\xi(X) \to \xi(\bar{X})$ and $\eta(X) \to \eta(\bar{X})$ are unchanged by the transformation at any material point $\bar{X} = X/L$. The elastic strain energy density becomes

$$\bar{W} = WL/(2\Upsilon) = \tfrac{1}{4}(1 - \xi)^2(\bar{\gamma} - \bar{\gamma}_0\varphi)^2. \tag{3.22}$$

Define the ratio R of twin boundary surface energy to fracture surface energy:

$$R = \Gamma/\Upsilon. \tag{3.23}$$

In dimensionless form, the total energy functional (3.11) becomes

$$\bar{\Psi}(\bar{v}, \eta, \xi) = \int_0^1 \left\{ \tfrac{1}{4}(1 - \xi)^2(\bar{\gamma} - \bar{\gamma}_0\varphi)^2 + \hat{\iota}R[6\eta^2(1 - \eta)^2/\bar{l} + \tfrac{3}{8}\bar{l}(\bar{\eta}')^2] + \tfrac{1}{2}\xi^2/\bar{l} \right.$$
$$\left. + \tfrac{1}{2}\bar{l}(\bar{\xi}')^2 \right\} d\bar{X}. \tag{3.24}$$

The Euler–Lagrange equation for stress equilibrium (3.13) becomes

$$\bar{P}'(\bar{X}) = \partial\bar{P}/\partial\bar{X} = 0 \Rightarrow \bar{P} = (1 - \xi)^2(\bar{\gamma} - \bar{\gamma}_0\varphi) = \text{constant}. \tag{3.25}$$

The Euler–Lagrange equation for fracture order parameter equilibrium, (3.15), reduces to

$$\tfrac{1}{2}(1 - \xi)(\bar{\gamma} - \bar{\gamma}_0\varphi)^2 - \xi/\bar{l} + \bar{l}\bar{\xi}'' - \hat{\iota}'R[\tfrac{3}{8}\bar{l}(\eta')^2 + 6\eta^2(1 - \eta)^2/\bar{l}] = 0. \tag{3.26}$$

The Euler–Lagrange equation for twinning order parameter equilibrium, (3.17), becomes

$$\tfrac{1}{2}(1 - \xi)^2\bar{\gamma}_0(\bar{\gamma} - \bar{\gamma}_0\varphi)\varphi' + \tfrac{3}{4}R\bar{l}[\hat{\iota}\bar{\eta}'' + \hat{\iota}'\bar{\eta}'\bar{\xi}'] - 12\hat{\iota}R\eta(1 - 3\eta + 2\eta^2)/\bar{l} = 0. \tag{3.27}$$

When the interpolation function $\varphi(\eta)$ is prescribed, solutions depend on no more than three dimensionless material parameters: length ratio $\bar{l}$, surface energy ratio R and twinning eigen-shear $\bar{\gamma}_0$.

3.2. *General coupled problem*

3.2.1. *Boundary conditions*

Both $\xi(X) \in [0, 1]$ and $\eta(X) \in [0, 1]$ can generally be nonzero and may possibly vary over domain Ω. Let $\bar{v}$ be the applied shear displacement to the right boundary of the domain $\bar{X} \in [0, 1]$, with the left end fixed with regards to displacement; i.e. considered are mechanical boundary conditions of the form

$$\bar{v}(0) = 0, \qquad \bar{v}(1) = \bar{v} = \int_0^1 \bar{\gamma} d\bar{X}, \tag{3.28}$$

along with vanishing order parameter gradients at the boundaries [i.e. $r = s = 0$ in (2.15) and (2.19)]:

$$\bar{\xi}'(0) = \bar{\xi}'(1) = 0, \qquad \bar{\eta}'(0) = \bar{\eta}'(1) = 0. \tag{3.29}$$

Several candidate solutions of (3.25), (3.26) and (3.27) are now analysed for these boundary conditions.

3.2.2. *Homogeneous elastic deformation*

Perhaps the simplest candidate solution is homogeneous elasticity, wherein

$$\eta = \xi = 0, \qquad \bar{P} = \bar{\gamma}, \qquad \bar{\Psi}(\bar{\gamma}, 0, 0) = \bar{\Psi}_E = \tfrac{1}{4}\bar{\gamma}^2. \tag{3.30}$$

Stress equilibrium (3.25) results in $\bar{\gamma} = \bar{\upsilon} = $ constant. Twinning order parameter equilibrium (3.27) at nonzero $\bar{\gamma}$ requires either $\gamma_0 = 0$ or $\varphi'(0) = 0$, the latter of which is satisfied by choice (2.35) in (2.37), for example. Fracture order parameter equilibrium (3.26) requires $\xi = \tfrac{1}{2}\bar{l}(1 - \xi)\bar{\gamma}^2 = 0$, which holds only at null applied deformation ($\bar{\upsilon} = \bar{\gamma} = 0$) or for $\bar{l} \to 0$. This is the same conclusion reported later in (3.65).

3.2.3. *Homogeneous damage followed by localized fracture or localized twinning*

Next consider homogeneous damage followed by localization to either fracture (Figure 1(f)) or twinning (Figure 1(a)). Prior to localization, no twinning occurs and ξ is spatially constant:

$$\xi(\bar{X}) = \xi_H = \text{constant}, \qquad \eta(\bar{X}) = 0. \tag{3.31}$$

Combining with equilibrium leads to constant shear stress $\bar{P}$ proportional to constant shear strain $\bar{\gamma} = \bar{\upsilon}$:

$$\bar{P} = (1 - \xi_H)^2 \bar{\gamma} = \text{constant}. \tag{3.32}$$

Twinning order parameter equilibrium (3.27) reduces to $(1 - \xi_H)^2 \bar{\gamma}_0 \bar{\gamma} \varphi'(0) = 0$, which at nonzero $\bar{\gamma}$ and $\xi_H < 1$ requires either $\gamma_0 = 0$ or $\varphi'(0) = 0$, the latter satisfied by choice (2.35) in (2.37). Prior to localization, fracture order parameter equilibrium (3.26) requires

$$(1 - \xi_H)\bar{\gamma}^2 - 2\xi_H/\bar{l} = 0, \tag{3.33}$$

which is identical to (3.61) of Section 3.3.2, with algebraic solution

$$\xi_H = \bar{\gamma}^2/(2/\bar{l} + \bar{\gamma}^2), \qquad \bar{P} = \bar{\gamma}/(1 + \bar{l}\bar{\gamma}^2/2)^2 \tag{3.34}$$

and total energy

$$\bar{\Psi}_H = \tfrac{1}{4}(1 - \xi_H)^2 \bar{\gamma}^2 + \tfrac{1}{2}\xi_H^2/\bar{l}. \tag{3.35}$$

Therefore, it follows that the homogeneously damaged state in Figure 1(d) is a feasible equilibrium solution consistent with the governing equations of the fully coupled theory. A lower bound for stability for this homogeneous solution is derived later in Section 3.3.3, with instability possible if $\bar{\gamma} > \sqrt{2/(3\bar{l})}$. However, transition to a localized stress-free and fully fractured state (Figure 1(e)) becomes energetically favorable if $\bar{\Psi}_H > \bar{\Psi}_F \approx 1$, which occurs for $\bar{\gamma} \gtrsim 2$ for small $\bar{l}$ as shown later in Figure 3(b). That such a locally fully failed state corresponds to a viable solution of the coupled boundary value problem is verified later in Section 3.3.4. However, transition from a homogeneously damaged condition to

this state may require reversibility of damage in regions outside the localized damage zone, which is physically unrealistic.

Upon transition from homogeneous damage to localized twinning, Equations (3.25)–(3.27) become

$$\bar{P} = (1 - \xi_H)^2(\bar{\gamma} - \bar{\gamma}_0\varphi) = \text{constant}, \tag{3.36}$$

$$\tfrac{1}{2}(1 - \xi_H)(\bar{\gamma} - \bar{\gamma}_0\varphi)^2 - \xi_H/\bar{l} - \hat{\imath}'(\xi_H)R[\tfrac{3}{8}\bar{l}(\eta')^2 + 6\eta^2(1 - \eta)^2/\bar{l}] = 0, \tag{3.37}$$

$$\tfrac{1}{2}(1 - \xi_H)^2\bar{\gamma}_0(\bar{\gamma} - \bar{\gamma}_0\varphi)\varphi' + \tfrac{3}{4}R\bar{l}\hat{\imath}(\xi_H)\bar{\eta}'' - 12R\eta(1 - 3\eta + 2\eta^2)\hat{\imath}(\xi_H)/\bar{l} = 0. \tag{3.38}$$

Simultaneous solution of the above three differential equations for ξ_H, $\eta(\bar{X})$ and $\bar{\gamma}(\bar{X})$ with nonzero shear stress $\bar{P}$ requires advanced numerical methods beyond the present scope. However, for the scenario shown in Figure 1(a) with vanishing shear stress ($\bar{P} = 0$), (3.36) is trivially satisfied, and (3.37) and (3.38) reduce to

$$-\xi_H/\bar{l} - \hat{\imath}'(\xi_H)R\left[\tfrac{3}{8}\bar{l}(\eta')^2 + 6\eta^2(1 - \eta)^2/\bar{l}\right] = 0, \tag{3.39}$$

$$\tfrac{3}{4}R\bar{l}[\hat{\imath}(\xi_H)\bar{\eta}''] - 12R\eta(1 - 3\eta + 2\eta^2)\hat{\imath}(\xi_H)/\bar{l} = 0. \tag{3.40}$$

Solution of (3.39) is difficult unless $\xi_H \to 0$ and $\hat{\imath}'(\xi_H) = 0$, which is the case studied later in Section 3.4.4. However, a stress-free solution satisfying the remaining governing equations can still be derived as follows. For $R > 0$ and $\xi_H < 1$, (3.40) can be reduced to (3.135):

$$\bar{\eta}'' - (32/\bar{l}^2)\eta^3 + (48/\bar{l}^2)\eta^2 - (16/\bar{l}^2)\eta = 0, \tag{3.41}$$

which has the inverse solution derived and evaluated in Section 3.4.4:

$$\bar{X}(\eta) = \bar{l}\int_0^1 \mathrm{d}\eta/[4\eta(1 - \eta)]. \tag{3.42}$$

The total energy of the stress-free, locally twinned domain becomes, using (3.140) in (3.24),

$$\bar{\Psi}_L = \int_0^1 \left\{\hat{\imath}(\xi_H)R[6\eta^2(1 - \eta)^2/\bar{l} + \tfrac{3}{8}\bar{l}(\bar{\gamma}')^2] + \tfrac{1}{2}\xi_H^2/\bar{l}\right\}\mathrm{d}\bar{X} = \hat{\imath}(\xi_H)R + \tfrac{1}{2}\xi_H^2/\bar{l}, \tag{3.43}$$

where the first term following the final equality accounts for twin boundary energy degraded by damage, and the second accounts for homogeneous damage. In the absence of homogeneous damage, $\hat{\imath} = 1$ and total energy (which then equals twice the normalized twin boundary surface energy) now takes the value of R rather than unity of (3.140) because of the difference in normalization factors used in (3.105) and (3.18). The homogeneously damaged, stressed and twin-free domain and the homogeneously damaged, unstressed domain with localized twinning have equal total energy when (3.35) and (3.43) are the same:

$$\bar{\Psi}_H = \bar{\Psi}_L \Leftrightarrow \tfrac{1}{4}(1 - \xi_H)^2\bar{\gamma}^2 = R\hat{\imath}(\xi_H). \tag{3.44}$$

Note that if $\hat{\imath}(\xi) = \hat{\phi}(\xi) = (1 - \xi)^2$, this equality is independent of the value of ξ_H, i.e. it then does not depend on the existence of homogeneous damage in the material. For this choice of $\hat{\imath}$, the ratio of energy for homogeneous damage, $\bar{\Psi}_H$ of (3.35), to the energy for localized twinning, $\bar{\Psi}_L$ of (3.43), is

$$\frac{\bar{\Psi}_H}{\bar{\Psi}_L} = \frac{(1 - \xi_H)^2\bar{\gamma}^2 + 2\xi_H^2/\bar{l}}{4(1 - \xi_H)^2R + 2\xi_H^2/\bar{l}}, \qquad \xi_H = \frac{\bar{\gamma}^2}{2/\bar{l} + \bar{\gamma}^2}. \tag{3.45}$$
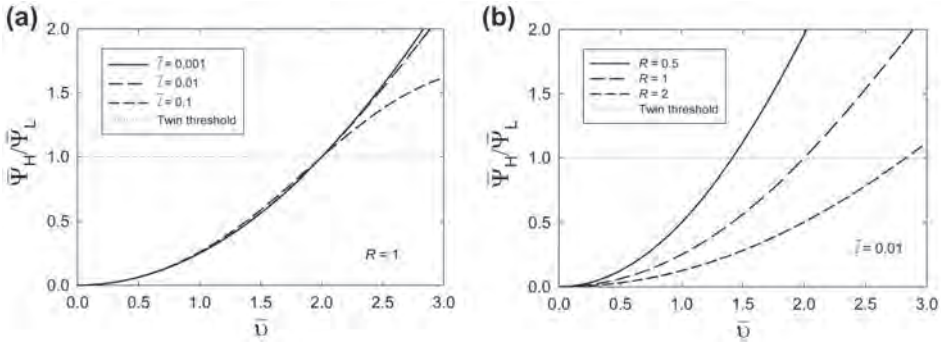
Figure 2. Ratio of energy for homogeneous damage $\bar{\Psi}_H$ to localized stress-free twinning energy $\bar{\Psi}_L$ for (a) equal twin boundary and fracture surface energies ($R = \Gamma/\Upsilon = 1$) and various dimensionless characteristic lengths $\bar{l}$ and (b) various ratios of twin boundary to fracture surface energies ($R = \Gamma/\Upsilon$) and fixed dimensionless characteristic length $\bar{l} = 0.01$. Dimensionless shear displacement is $\bar{\upsilon}$. Transition from homogeneous damage to localized stress-free twinning is energetically favourable if $\bar{\Psi}_H/\bar{\Psi}_L \gtrsim 1$.

This ratio is shown in Figure 2(a) for various length parameters $\bar{l}$ and $R = 1$, and in Figure 2(b) for various surface energy ratios R and fixed $\bar{l} = 0.01$. A transition from homogeneous damage to localized twinning occurs when applied displacement $\bar{\upsilon} = \bar{\gamma}$ is such that the ratio in the first equality of (3.45) exceeds unity, which corresponds to intersection of the curves in Figure 2(a) or (b) with the dotted line denoted "twin threshold". The intersection point is insensitive to $\bar{l}$ as evident from Figure 2(a), but logically occurs at lower applied displacement $\bar{\upsilon}$ for smaller R, which corresponds to relatively lower twin boundary surface energy (Figure 2(b)). For the choice $\hat{\iota}(\xi) = \hat{\phi}(\xi)$ used here, or any other choice with $\xi_H = 0$ and $\hat{\iota}(0) = 1$, transition from homogeneous deformation to localized stress-free twinning becomes energetically favourable for

$$\bar{\upsilon} = \bar{\gamma} \geq 2\sqrt{R}. \tag{3.46}$$

This can be compared with the criterion derived later in Section 3.3.4 for transition from homogeneous elastic deformation to localized stress-free fracture:

$$\bar{\upsilon} = \bar{\gamma} \geq 2 \quad (\bar{l} \lesssim 0.01). \tag{3.47}$$

Comparison of the two criteria leads to the conclusion that localized twinning should occur at earlier applied shear displacement $\bar{\upsilon}$ than localized mode II fracture for $R < 1$, and the converse for $R > 1$, if the state with lowest total energy is preferred. It should be recalled, however, that the state with total energy (3.43) is generally a nonequilibrium state with regards to the fracture parameter ξ since (3.39) is not necessarily always satisfied for the fully coupled model when $\xi_H > 0$. However, recalling that (3.39) is satisfied if $\xi_H = 0$ [so long as $\hat{\iota}'(0) = 0$], the above transition criteria are fully valid for evaluating abrupt localized fracture or localized twinning from an initially undamaged state.

3.3. *Fracture in simple shear*

Considered in Section 3.3 is reduction of the general theory of Section 3.1 to the case where fracture/damage may occur but twinning is prohibited. In terms of order parameters, this implies $\eta(X) = 0 \forall X \in \Omega$, while $\xi(X) \in [0, 1]$ can vary over domain Ω. In terms of material properties, twinning would be prohibited by setting $\gamma_0 \to 0$ and Γ very large, such that Ψ of (2.9) would be penalized unconditionally for any nonzero η field.

3.3.1. *Reduced governing equations*

Since no twinning occurs, $\varphi(\eta) = \varphi(0) = 0$, $\boldsymbol{F}^\eta(\eta) = \boldsymbol{F}^\eta(0) = \boldsymbol{1}$ and $\boldsymbol{F} = \boldsymbol{F}^{\mathrm{E}}$ everywhere in Ω. Thus, the elastic deformation tensor of (2.6) and (3.7) is, in matrix form, and with trace:

$$[\boldsymbol{C}] = \begin{bmatrix} 1 + \gamma^2 & \gamma & 0 \\ \gamma & 1 & 0 \\ 0 & 0 & 1 \end{bmatrix}, \qquad \mathrm{tr}\boldsymbol{C} = 3 + \gamma^2. \tag{3.48}$$

As in Section 3.1, assume $\zeta = 0$ such that $\hat{\phi}(\xi) = (1 - \xi)^2$. Strain energy density of (2.20) or (3.8) then reduces to

$$W[\gamma(X), \xi(X)] = \tfrac{1}{2}\mu(\mathrm{tr}\boldsymbol{C} - 3) = \tfrac{1}{2}\mu_0(1 - \xi)^2\gamma^2. \tag{3.49}$$

Again denoting the length parameter h by l, (2.30)–(2.32) combine and reduce to (3.9). The energy functional (2.9) or (3.11) becomes, per unit cross-sectional area,

$$\Psi(v, \xi) = \int_0^L c\left[\tfrac{1}{2}\mu_0(1 - \xi)^2\gamma^2 + \Upsilon\xi^2/l + \Upsilon l(\xi')^2\right]\mathrm{d}X. \tag{3.50}$$

From (3.12), or (2.13) and (2.20) with $J = 1$, stress obeys $\boldsymbol{P} = \mu(\boldsymbol{F} - \boldsymbol{F}^{-\mathrm{T}})$, with nonzero components

$$P(X) = P_{xY} = P_{yX} = \mu_0(1 - \xi)^2\gamma. \tag{3.51}$$

The Euler–Lagrange equation for stress equilibrium, (3.13), applies where now specifically

$$P'(X) = \partial P/\partial X = 0 \Rightarrow P/\mu_0 = (1 - \xi)^2\gamma = \text{constant}. \tag{3.52}$$

The conjugate driving force for fracture of (2.34) or (3.14) is

$$\varsigma(X) = \partial W/\partial \xi = -\mu_0(1 - \xi)\gamma^2. \tag{3.53}$$

The Euler–Lagrange equation for order parameter equilibrium, (2.34) or (3.15), reduces to

$$\mu_0(1 - \xi)\gamma^2 - 2\Upsilon\xi/l + 2\Upsilon l\xi'' = 0. \tag{3.54}$$

Similar to [14,31], apply definitions in (3.18)–(3.20). The total energy in (3.24) or (3.50) becomes

$$\bar{\Psi}(\bar{v}, \xi) = \int_0^1 \left[\tfrac{1}{4}(1 - \xi)^2\bar{\gamma}^2 + \tfrac{1}{2}\xi^2/\bar{l} + \tfrac{1}{2}\bar{l}(\bar{\xi}')^2\right]\mathrm{d}\bar{X}. \tag{3.55}$$

The Euler–Lagrange equation for stress equilibrium (3.25) or (3.52) becomes

$$\bar{P}'(\bar{X}) = \partial\bar{P}/\partial\bar{X} = 0 \Rightarrow \bar{P} = (1 - \xi)^2\bar{\gamma} = \text{constant}. \tag{3.56}$$

The Euler–Lagrange equation for order parameter equilibrium (3.26) or (3.54) likewise becomes

$$\tfrac{1}{2}(1 - \xi)\bar{\gamma}^2 - \xi/\bar{l} + \bar{l}\bar{\xi}'' = 0. \tag{3.57}$$

Solutions now depend on only one material parameter, the dimensionless length ratio $\bar{l}$.

3.3.2. *Homogeneous elasticity and damage*

Solutions to the problem outlined in Section 3.3.1 are now sought for which damage is spatially homogeneous:

$$\xi(\bar{X}) = \xi_H = \text{constant}, \qquad \bar{\xi}'(\bar{X}) = \bar{\xi}''(\bar{X}) = 0. \tag{3.58}$$

A subset of this class of solutions is shown in Figure 1(b), for which the domain remains perfectly elastic and $\xi = 0 \forall \bar{X} \in [0, 1]$; an example of homogeneous damage with $0 < \xi < 1$ is shown in Figure 1(d). Stress is constant by (3.56); it follows from (3.19) and (3.58) that strain $\bar{\gamma}$ is also constant:

$$\bar{P} = (1 - \xi_H)^2\bar{\gamma} = \text{constant} \Rightarrow \bar{\gamma} = \bar{P}/(1 - \xi_H)^2 = \text{constant}. \tag{3.59}$$

Let the domain be fixed at $\bar{X} = 0$, and denote by $\bar{\upsilon}$ the shear displacement at $\bar{X} = 1$:

$$\bar{\upsilon}(0) = 0, \qquad \bar{\upsilon}(1) = \bar{\upsilon} = \int_0^1 \bar{\gamma}\,\mathrm{d}\bar{X} = \bar{\gamma}\int_0^1 \mathrm{d}\bar{X} = \bar{\gamma}. \tag{3.60}$$

Using (3.58), order parameter equilibrium (3.57) requires

$$(1 - \xi_H)\bar{\gamma}^2 = 2\xi_H/\bar{l}, \tag{3.61}$$

which has the algebraic solution

$$\xi_H = \bar{\gamma}^2/(2/\bar{l} + \bar{\gamma}^2), \qquad \bar{P} = \bar{\gamma}/(1 + \bar{l}\bar{\gamma}^2/2)^2. \tag{3.62}$$

Dimensionless stress $\bar{P}$ is shown in Figure 3(a), noting from (3.60) that $\bar{\upsilon} = \bar{\gamma}$ in this case. Under load control (i.e. imposed nonzero $\bar{P}$), the solution is nonunique except at the load corresponding to maximum stress since two strain states can produce the same stress state. Stress attains a maximum value $\bar{P}_C$ at shear $\bar{\gamma}_C$:

$$\mathrm{d}\bar{P}/\mathrm{d}\bar{\gamma} = 0 \Rightarrow \bar{\gamma}_C = \sqrt{2/(3\bar{l})}, \quad \bar{P}_C = \tfrac{3}{16}\sqrt{6/\bar{l}}. \tag{3.63}$$

The maximum stress is achieved at $\xi_H = \tfrac{1}{4}$ regardless of $\bar{l}$, so long as $\bar{l} > 0$. Total energy (3.55) becomes

$$\bar{\Psi}_H = \bar{\Psi}[\bar{\gamma}, \xi_H(\bar{\gamma})] = \int_0^1 \left[\tfrac{1}{4}(1 - \xi_H)^2\bar{\gamma}^2 + \tfrac{1}{2}\xi_H^2/\bar{l}\right]\mathrm{d}\bar{X} = \tfrac{1}{4}(1 - \xi_H)^2\bar{\gamma}^2 + \tfrac{1}{2}\xi_H^2/\bar{l}. \tag{3.64}$$

At maximum stress conditions (3.63), $\bar{\Psi}_H = 1/(8\bar{l})$. Total energy $\bar{\Psi}_H$ is shown in Figure 3(b); as will be derived later in Section 3.3.4, the total energy associated with localized stress-free fracture–see Figure 1(e) and the dotted horizontal line in Figure 3(b) – is $\bar{\Psi}_L \approx 1$ for $\bar{l} \lesssim 0.1$, regardless of applied displacement. As the characteristic length shrinks to zero, the purely elastic homogeneous solution is recovered:

$$(\xi_H, \bar{P}, \bar{\Psi}) \to (0, \bar{\gamma}, \bar{\gamma}^2/4) \quad \text{as } \bar{l} \to 0. \tag{3.65}$$
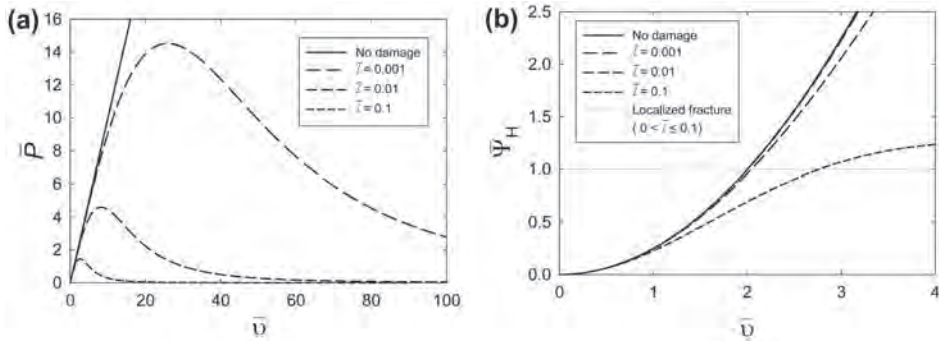
Figure 3. Homogeneous analytical solution for (a) dimensionless stress $\bar{P}$ vs. dimensionless shear displacement $\bar{\upsilon}$ and (b) dimensionless energy $\bar{\Psi}_H$ vs. $\bar{\upsilon}$. Dimensionless characteristic length (interfacial width) is $\bar{l}$. Localized stress-free fracture becomes energetically favourable to homogeneous damage when $\bar{\Psi}_H > \bar{\Psi}_F \gtrsim 1$.

3.3.3. *Stability*

Stability, or lack thereof, of the homogeneous solution derived in Section 3.3.2, is now analysed. The present analysis extends previous studies [14,30,32–35], and most closely resembles the dimensionless analysis in [31]. In contrast to these prior works that focused on stability of models involving linear elasticity and one-dimensional tensile loading, the present analysis considers nonlinear elasticity and finite simple shear.

A family of candidate solutions is now introduced, where α is a scalar parameter (i.e. perturbation) whose magnitude denotes deviation from the homogeneous solution ξ_H:

$$\xi = \xi(\bar{X}, \alpha), \quad \xi(\bar{X}, 0) = \xi_H; \qquad \bar{\upsilon} = \bar{\upsilon}(\bar{X}, \alpha), \quad \bar{\gamma}(\bar{X}, \alpha) = \partial \bar{\upsilon}/\partial \bar{X}. \tag{3.66}$$

Displacement boundary conditions are imposed, and candidate solutions are required to obey the same such boundary conditions imposed for the homogeneous solution:

$$\bar{\upsilon}(0, \alpha) = \bar{\upsilon}(0, 0) = 0, \qquad \bar{\upsilon}(1, \alpha) = \bar{\upsilon}(1, 0) = \bar{\upsilon} = \int_0^1 \bar{\gamma}(\bar{X}, \alpha) d\bar{X}. \tag{3.67}$$

The candidate solutions for ξ are further expected to have vanishing order parameter gradients $\bar{\xi}' = \partial \xi(\bar{X}, \alpha)/\partial \bar{X}$ at the endpoints (such a requirement is trivially satisfied by the homogeneous solution):

$$\bar{\xi}'(0, \alpha) = \bar{\xi}'(1, \alpha) = 0. \tag{3.68}$$

Define the following integral function of parameter α:

$$\vartheta(\alpha) = \int_0^1 d\bar{X}/[1 - \xi(\bar{X}, \alpha)]^2. \tag{3.69}$$

Recalling from (3.51) and (3.56) that shear stress obeys $\bar{P} = (1 - \xi)^2 \bar{\gamma}$ and is independent of $\bar{X}$,

$$\bar{\upsilon} = \int_0^1 \bar{\gamma}(\bar{X}, \alpha) d\bar{X} = \bar{P}(\alpha) \int_0^1 d\bar{X}/[1 - \xi(\bar{X}, \alpha)]^2 = \bar{P}(\alpha) \vartheta(\alpha). \tag{3.70}$$

The following relations then can be derived directly:

$$\bar{P}(\alpha) = \bar{\upsilon}/\vartheta(\alpha), \qquad \bar{\gamma}(\bar{X}, \alpha) = \bar{\upsilon}/\{\vartheta(\alpha)[1 - \xi(\bar{X}, \alpha)]^2\}; \tag{3.71}$$

$$\frac{\mathrm{d}\vartheta(\alpha)}{\mathrm{d}\alpha} = \int_0^1 \frac{2}{[1 - \xi(\bar{X}, \alpha)]^3} \frac{\partial \xi(\bar{X}, \alpha)}{\partial \alpha} \mathrm{d}\bar{X}; \tag{3.72}$$

$$\frac{\mathrm{d}^2\vartheta(\alpha)}{\mathrm{d}\alpha^2} = \int_0^1 \frac{2}{[1 - \xi(\bar{X}, \alpha)]^3} \frac{\partial^2 \xi(\bar{X}, \alpha)}{\partial \alpha^2} \mathrm{d}\bar{X} + \int_0^1 \frac{6}{[1 - \xi(\bar{X}, \alpha)]^4} \left[\frac{\partial \xi(\bar{X}, \alpha)}{\partial \alpha} \right]^2 \mathrm{d}\bar{X}. \tag{3.73}$$

The total energy of (3.55) in terms of parameter α is

$$\bar{\Psi}(\alpha) = \int_0^1 [\tfrac{1}{4}\bar{P}\bar{\gamma} + \tfrac{1}{2}\xi^2/\bar{l} + \tfrac{1}{2}\bar{l}(\bar{\xi}')^2]\mathrm{d}\bar{X} = \tfrac{1}{2}\int_0^1 \bar{\upsilon}^2/(2\vartheta) + \xi^2/\bar{l} + \bar{l}(\bar{\xi}')^2]\mathrm{d}\bar{X}. \tag{3.74}$$

The first variation of total energy is, upon integration by parts and use of boundary conditions in (3.68),

$$\delta\bar{\Psi}(\alpha) = -\frac{\bar{\upsilon}^2}{4\vartheta^2} \int_0^1 \frac{\mathrm{d}\vartheta}{\mathrm{d}\alpha} \mathrm{d}\bar{X}\delta\alpha + \int_0^1 \left(\frac{\xi}{\bar{l}} - \bar{l}\bar{\xi}'' \right) \frac{\partial \xi}{\partial \alpha} \mathrm{d}\bar{X}\delta\alpha + \left(\bar{l}\bar{\xi}' \frac{\partial \xi}{\partial \alpha} \right)\bigg|_0^1$$
$$= -\frac{\bar{\upsilon}^2}{2\vartheta^2} \int_0^1 \frac{1}{(1 - \xi)^3} \frac{\partial \xi}{\partial \alpha} \mathrm{d}\bar{X}\delta\alpha + \int_0^1 \left(\frac{\xi}{\bar{l}} - \bar{l}\bar{\xi}'' \right) \frac{\partial \xi}{\partial \alpha} \mathrm{d}\bar{X}\delta\alpha. \tag{3.75}$$

Noting for the homogeneous solution ($\alpha = 0$) that

$$\bar{\xi}''(\bar{X}, 0) = 0, \qquad \vartheta(0) = 1/(1 - \xi_H)^2, \tag{3.76}$$

and consulting (3.61), the first variation (3.75) vanishes identically, as it should for an equilibrium state:

$$\delta\bar{\Psi}(0) = -\frac{1}{2}\int_0^1 \bar{\gamma}^2(1 - \xi_H)\frac{\partial \xi}{\partial \alpha}\mathrm{d}\bar{X}\delta\alpha + \int_0^1 \frac{\xi_H}{\bar{l}}\frac{\partial \xi}{\partial \alpha}\mathrm{d}\bar{X}\delta\alpha = 0. \tag{3.77}$$

Appealing to (3.72) and (3.73), the second variation of (3.74) at $\alpha = 0$ is computed as

$$\frac{\delta^2\bar{\Psi}}{\delta\alpha^2}(0) = 2\bar{\upsilon}^2 \left(\int_0^1 \frac{\partial \xi}{\partial \alpha}\mathrm{d}\bar{X} \right)^2 + \bar{l}\int_0^1 \left(\frac{\partial \bar{\xi}'}{\partial \alpha} \right)^2 \mathrm{d}\bar{X} + \left(\frac{1}{\bar{l}} - \frac{3\bar{\upsilon}^2}{2} \right)\int_0^1 \left(\frac{\partial \xi}{\partial \alpha} \right)^2 \mathrm{d}\bar{X}. \tag{3.78}$$

As discussed in [30], $\frac{\delta^2\bar{\Psi}}{\delta\alpha^2}(0) \geq 0$ is necessary for stability of the homogeneous solution, and $\frac{\delta^2\bar{\Psi}}{\delta\alpha^2}(0) > 0$ is sufficient for stability of the homogeneous solution. Noting that the first two terms on the right of (3.78) are always nonnegative, and noting for the homogeneous solution that $\bar{\upsilon} = \bar{\gamma}$, a lower bound for the unstable domain in terms of applied shear strain is determined by the third term on the right of (3.78):

$$\bar{\gamma} > \sqrt{2/(3\bar{l})} = \bar{\gamma}_C. \tag{3.79}$$

Accordingly, the homogeneous solution can become unstable under Displacement-controlled loading when maximum uniform stress $\bar{P}_C$ of (3.63) is exceeded. Exact stability conditions for the analogous tensile problem are derived in [35], where it is shown that terms analogous to the first two integrals on the right of (3.78) become significant only for relatively large

$\bar{l} \gtrsim 0.4$, in which case the maximum strain possible in the stable domain can be larger. Otherwise, for the more physically realistic case of thinner crack boundaries (i.e. for small $\bar{l}$), (3.79) becomes exact.

3.3.4. *Localized complete fracture*

Considered next is the problem shown in Figure 1(e): a stress-free domain with localized damage concentrated at the midpoint. Applied displacement $\bar{\upsilon} = \bar{v}(1)$ may take any value since $\bar{\gamma}$ may be unbounded without energetic consequence where the material is fully fractured/degraded. Mechanical loading conditions are

$$\bar{P} = [1 - \bar{\xi}(\bar{X})]^2 \bar{\gamma}(\bar{X}) = 0, \qquad \bar{v}(0) = 0. \tag{3.80}$$

This implies $\bar{\gamma}(\bar{X}) = 0 \forall \xi(\bar{X}) < 1$. Boundary and symmetry conditions on the order parameter are

$$\bar{\xi}'(0) = \bar{\xi}'(1) = 0, \qquad \xi\left(\tfrac{1}{2}\right) = 1. \tag{3.81}$$

The vanishing order parameter gradient boundary condition implies conjugate traction $s = 0$ in (2.15) and (2.19). Stress equilibrium is trivially satisfied. Order parameter equilibrium (3.57) becomes the linear, homogeneous second-order differential equation

$$\bar{\xi}'' - \xi/\bar{l}^2 = 0, \tag{3.82}$$

which has the immediate solution

$$\xi(\bar{X}) = c_1 e^{\bar{X}/\bar{l}} + c_2 e^{-\bar{X}/\bar{l}}; \tag{3.83}$$

$$c_1 = c_2 = 1/[e^{1/(2\bar{l})} + e^{-1/(2\bar{l})}] \quad \text{for } \bar{X} \leq \tfrac{1}{2}$$
$$c_1 = 1/[e^{1/(2\bar{l})} + e^{3/(2\bar{l})}], \quad c_2 = 1/[e^{-1/(2\bar{l})} + e^{-3/(2\bar{l})}] \quad \text{for } \bar{X} \geq \tfrac{1}{2}. \tag{3.84}$$

The dimensionless total energy functional in (3.55) is then

$$\bar{\Psi}_F = \tfrac{1}{2} \int_0^1 [\xi^2/\bar{l} + \bar{l}(\bar{\xi}')^2] d\bar{X} = \int_0^{1/2} [\xi^2/\bar{l} + \bar{l}(\bar{\xi}')^2] d\bar{X} = \frac{e^{1/\bar{l}} + e^{-1/\bar{l}}}{[e^{1/(2\bar{l})} + e^{-1/(2\bar{l})}]^2}. \tag{3.85}$$

A direct calculation verifies that $\bar{\Psi}_F \approx 1$ for $\bar{l} \lesssim 0.1$, as depicted by the horizontal dotted line in Figure 3(b). As is evident from this figure, for small $\bar{l}$, the localized stress-free solution has greater total energy than the homogeneous damage solution ($\bar{\Psi}_F > \bar{\Psi}_H$) for applied shear $\bar{\upsilon} \lesssim 2$. However, stability of the homogeneous elastic solution in the context of the perturbation analysis of Section 3.3.3 holds for $\bar{\upsilon} \lesssim \gamma_C = \sqrt{2/(3\bar{l})}$. For example, taking $\bar{l} = 0.01$, stability holds for $\bar{\upsilon} \lesssim 8$, but the homogeneous solution of Section 3.3.2 represents a local minimum energy configuration (i.e. is in fact metastable) for $2 \lesssim \bar{\upsilon} \lesssim 8$.

Verification is straightforward that this candidate solution involving stress-free, localized fracture, in the absence of twinning, is valid for the fully coupled theory of Section 3.2. Since $\eta(\bar{X}) = 0$, $\bar{P} = (1 - \xi)^2 \bar{\gamma} = 0 \Rightarrow \bar{\gamma} = 0 \forall \xi < 1$. Twinning order parameter equilibrium (3.27) reduces to $(1 - \xi)^2 \bar{\gamma}_0 \bar{\gamma} \varphi'(0) = 0$, which is identically satisfied by $\bar{P} = 0$. Fracture order parameter equilibrium (3.26) reduces to (3.82); the solution for $\xi(\bar{X})$ is (3.83) with integration constants (3.84). The total energy of this stress-free domain with localized complete fracture $\left(\xi = 1 \text{ at } \bar{X} = \tfrac{1}{2}\right)$ is given by (3.85), i.e. in notation of Section 3.2.3, $\bar{\Psi}_L = \bar{\Psi}_F \approx 1$ for $\bar{l} \leq 0.1$.

3.3.5. *Inhomogeneous damage*

Solutions are sought to the shear problem wherein damage (i.e. ξ) may be nonuniform over domain [0, 1]; see Figure 1(f). The solution procedure is similar to that described elsewhere for tensile loading [14,31,32].

The loading parameter is stress $\bar{P}$, constant over the domain according to (3.56). Boundary conditions are imposed so that the homogeneous solution of Section 3.3.2 is also a solution to the present problem:

$$\xi(0) = \xi(1) = \xi_H(\bar{P}), \qquad \bar{\xi}'(0) = \bar{\xi}'(1) = 0. \tag{3.86}$$

Here, $\xi_H(\bar{P})$ is the value of the order parameter in the corresponding homogeneous solution during the loading phase prior to instability $\left(\xi_H \leq \frac{1}{4}\right)$ and is obtained by simultaneous solution of (3.62) with $\bar{P} \leq \bar{P}_C$ imposed. The following symmetry conditions are also imposed:

$$\bar{\xi}'\left(\tfrac{1}{2}\right) = 0, \qquad \bar{\xi}\left(\tfrac{1}{2} - \bar{X}\right) = \bar{\xi}\left(\tfrac{1}{2} + \bar{X}\right). \tag{3.87}$$

The displacement at the right end, $\bar{v}(1) = \bar{v}$, can be determined as an outcome of the solution.

The Euler–Lagrange equation for order parameter equilibrium (3.57) becomes, in terms of $\bar{P} = (1 - \xi)^2 \bar{\gamma} = $ constant and ξ,

$$\tfrac{1}{2} \bar{P}^2 / (1 - \xi)^3 - \xi / \bar{l} + \bar{l} \bar{\xi}'' = 0. \tag{3.88}$$

Its solution is facilitated by the following change of variables:

$$s(\bar{X}) = 1 - \xi(\bar{X}), \qquad s'(\bar{X}) = -\bar{\xi}'(\bar{X}), \qquad s''(\bar{X}) = -\bar{\xi}''(\bar{X}). \tag{3.89}$$

In terms of s and $\bar{P}$, (3.88) becomes

$$\bar{l}^2 s'' + \tfrac{1}{2} \bar{P}^2 \bar{l} / s^3 + s - 1 = 0. \tag{3.90}$$

Using the identities

$$-\frac{d}{ds}\left(\frac{1}{4s^2}\right) = \frac{1}{2s^3}, \qquad \frac{d}{ds}\left[\frac{(s')^2}{2}\right] = s'', \tag{3.91}$$

Equation (3.90) can be written

$$\frac{d}{ds}\left[\frac{\bar{l}^2 (s')^2}{2}\right] - \frac{d}{ds}\left(\frac{\bar{P}^2 \bar{l}}{4s^2}\right) + \frac{d}{ds}\left(\frac{s^2}{2}\right) - \frac{d}{ds}(s) = 0. \tag{3.92}$$

Defining $s\left(\tfrac{1}{2}\right) = s_M = 1 - \xi\left(\tfrac{1}{2}\right)$ and noting that $s'\left(\tfrac{1}{2}\right) = 0$ from (3.87), integration of (3.92) over domain $[s_M, s(\bar{X})]$ corresponding to right half $\bar{X} \geq \tfrac{1}{2}$ results in

$$\bar{l}^2 (s')^2 / 2 - \bar{P}^2 \bar{l} / \left(4s^2\right) + s^2/2 - s = -\bar{P}^2 \bar{l} / \left(4s_M^2\right) + s_M^2/2 - s_M. \tag{3.93}$$

Defining $s_H = 1 - \xi_H$, and noting boundary conditions $s(1) = s_H$ and $s'(1) = (ds/d\bar{X})(1) = 0$, the following equation can be solved numerically for s_M for a given $\bar{P}$:

$$\bar{P}^2 \bar{l} / \left(4s_M^2\right) - s_M^2/2 + s_M = \bar{P}^2 \bar{l} / \left(4s_H^2\right) - s_H^2/2 + s_H. \tag{3.94}$$
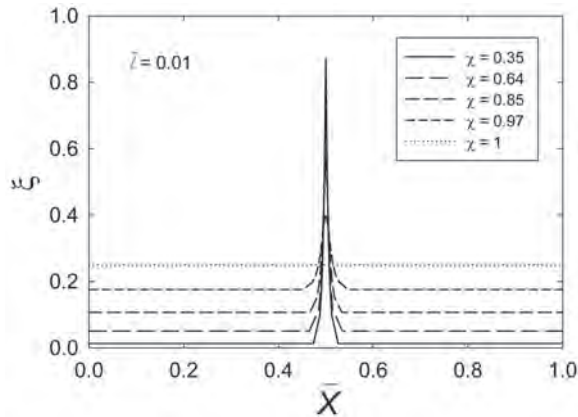
Figure 4. Inhomogeneous numerical solution for order parameter ξ vs. dimensionless coordinate $\bar{X}$. Dimensionless characteristic length is $\bar{l}$. Ratio of applied stress to critical stress at instability is $\chi = \bar{P}/\bar{P}_C$.

Inversion of (3.93) leads to a differential equation for $\bar{X}(s)$:

$$\mathrm{d}\bar{X}/\mathrm{d}s = 1/s' = (\bar{l}/\sqrt{2}) \left[\bar{P}^2\bar{l}/(4s_M^2) + s_M^2/2 - s_M + \bar{P}^2\bar{l}/(4s^2) - s^2/2 + s \right]^{-1/2}; \tag{3.95}$$

integration results in

$$\bar{X}(s) = (\bar{l}/\sqrt{2}) \int_{1/2}^1 \left[\bar{P}^2\bar{l}/(4s_M^2) + s_M^2/2 - s_M + \bar{P}^2\bar{l}/(4s^2) - s^2/2 + s \right]^{-1/2} \mathrm{d}s. \tag{3.96}$$

This can be numerically evaluated and then inverted to provide the order parameter profile $\xi(\bar{X}) = 1 - s(\bar{X})$ for $\bar{X} \in \left[\frac{1}{2}, 1\right]$; the profile for $\bar{X} \le \frac{1}{2}$ is then obtained by applying symmetry conditions (3.87). Results are shown in Figure 4 for $\bar{l} = 0.01$, where $\chi = \bar{P}/\bar{P}_C$ is the applied stress normalized by critical stress of (3.63). As the applied stress decreases (increases), fracture in the inhomogeneous solution becomes more localized (diffuse). The total energy and right side displacement are obtained by numerically evaluating the integrals

$$\bar{\Psi}(\bar{P}) = \int_0^1 [\tfrac{1}{4}\bar{P}\bar{\gamma} + \tfrac{1}{2}\xi^2/\bar{l} + \tfrac{1}{2}\bar{l}(\bar{\xi}')^2]\mathrm{d}\bar{X}, \qquad \bar{v}(\bar{P}) = \int_0^1 \bar{\gamma}\,\mathrm{d}\bar{X} = \int_0^1 [\bar{P}/(1-\xi)^2]\mathrm{d}\bar{X}. \tag{3.97}$$

Results are compared with those of the homogeneous solution of Section 3.2 (i.e. $\bar{\Psi}_H$ and $\bar{v}_H$) in Table 1. For $\chi < 1$, the total energy and right side shear displacement of the inhomogeneous solution exceed that of the homogeneous solution; as $\chi \to 1$, the inhomogeneous solution degenerates to the homogeneous solution.

3.4. *Twinning in simple shear*

Considered in Section 3.4 is reduction of the general theory of Section 3.2 to the case where deformation twinning may occur, but fracture is prohibited. This implies $\xi(X) = 0 \forall X \in \Omega$, while $\eta(X) \in [0, 1]$ can vary spatially over domain Ω. In terms of material properties,

Table 1. Comparison of total energy and displacement between inhomogeneous and homogeneous solutions (nonlinear phase field fracture model) under load control; ξ_M is the maximum value of the order parameter in the inhomogeneous solution, and ξ_H is the homogeneous order parameter.

χ	$\bar{\Psi}$	$\bar{\Psi}_H$	$\bar{\upsilon}$	$\bar{\upsilon}_H$	ξ_M	ξ_H
0.35	1.3	0.7	1.8	1.6	0.87	0.01
0.64	3.1	2.5	3.5	3.3	0.72	0.05
0.85	5.8	5.4	5.1	4.9	0.57	0.11
0.97	9.1	8.8	6.7	6.5	0.40	0.18
1	12.5	12.5	8.2	8.2	0.25	0.25

fracture/damage would be prohibited by setting Υ very large and $\hat{\phi} = \hat{\iota} = 1$, such that Ψ of (2.9) would be penalized unconditionally for any nonzero ξ field.

3.4.1. *Reduced governing equations*

Twinning deformation (2.5) is of the form in (3.5), and the elastic deformation tensor of (2.6) is identical to that in (3.7). Noting that in the absence of damage, $\mu = \mu_0$, $\phi = 0$ and $\hat{\phi} = \hat{\iota} = 1$, strain energy density of (2.20) or (3.8) reduces to

$$W[\gamma(X), \eta(X)] = \tfrac{1}{2}\mu_0(\text{tr}\boldsymbol{C} - 3) = \tfrac{1}{2}\mu_0(\gamma - \gamma_0\varphi)^2. \tag{3.98}$$

Equations (2.26)–(2.28) or (3.10) reduce to

$$f_0[\eta(X)] = (12\Gamma/l)\eta^2(1 - \eta)^2, \qquad \boldsymbol{\kappa} : \nabla\eta \otimes \nabla\eta = (3\Gamma l/4)[\eta'(X)]^2. \tag{3.99}$$

The energy functional (2.9) or (3.11) becomes, per unit cross-sectional area,

$$\Psi(v, \eta) = \int_0^L \left[\tfrac{1}{2}\mu_0(\gamma - \gamma_0\varphi)^2 + 12\Gamma\eta^2(1 - \eta)^2/l + \tfrac{3}{4}\Gamma l(\eta')^2 \right] dX. \tag{3.100}$$

From (3.12), or from (2.13) and (2.20) with $J = 1$, the stress tensor reduces to $\boldsymbol{P} = \mu(\boldsymbol{F}^E - \boldsymbol{F}^{E-T})\boldsymbol{F}^{\eta-T}$. The only resulting nonzero components are

$$P(X) = P_{xY} = P_{yX} = \mu_0(\gamma - \gamma_0\varphi), \qquad P_{yY}(X) = -\mu_0(\gamma - \gamma_0\varphi)\gamma_0\varphi. \tag{3.101}$$

The Euler–Lagrange equation for stress equilibrium (3.13) is now

$$P'(X) = \partial P/\partial X = 0 \Rightarrow P/\mu_0 = \gamma - \gamma_0\varphi = \text{constant}. \tag{3.102}$$

The conjugate driving force for twinning of (2.33) or (3.16) reduces to

$$\tau(X) = \partial W/\partial\eta = -\mu_0\gamma_0(\gamma - \gamma_0\varphi)\varphi', \tag{3.103}$$

where $\varphi' = d\varphi/d\eta$. The Euler–Lagrange equation for order parameter equilibrium in (2.33) or (3.17) is now

$$\tfrac{3}{2}\Gamma l\eta'' - 24\Gamma\eta(1 - 3\eta + 2\eta^2)/l + \mu_0\gamma_0(\gamma - \gamma_0\varphi)\varphi' = 0. \tag{3.104}$$

Similar to Section 3.1, dimensionless variables denoted with overbars are used in Section 3.4; however, twin boundary surface energy Γ, rather than fracture energy Υ, is applied for normalization here [(3.21) still holds]:

$$\bar{X} = X/L, \qquad \bar{l} = l/L, \qquad \bar{v} = v\sqrt{\mu_0/(\Gamma L)}, \qquad \bar{\mu}_0 = 1, \qquad \bar{\Psi} = \Psi L/(2\Gamma); \tag{3.105}$$

$$\bar{\gamma} = \partial\bar{v}/\partial\bar{X} = \gamma\sqrt{\mu_0 L/\Gamma}, \qquad \bar{\gamma}_0 = \gamma_0\sqrt{\mu_0 L/\Gamma}, \qquad \bar{P} = P\sqrt{L/(\mu_0\Gamma)} = \bar{\gamma} - \bar{\gamma}_0\varphi. \tag{3.106}$$

The total energy functional (3.24) or (3.100) becomes, in normalized form,

$$\bar{\Psi}(\bar{v}, \eta) = \int_0^1 \left[\tfrac{1}{4}(\bar{\gamma} - \bar{\gamma}_0\varphi)^2 + 6\eta^2(1 - \eta)^2/\bar{l} + \tfrac{3}{8}\bar{l}(\bar{\eta}')^2 \right] d\bar{X}. \tag{3.107}$$

The Euler–Lagrange equation for stress equilibrium (3.25) or (3.102) becomes

$$\bar{P}'(\bar{X}) = \partial\bar{P}/\partial\bar{X} = 0 \Rightarrow \bar{P} = \bar{\gamma} - \bar{\gamma}_0\varphi = \text{constant}. \tag{3.108}$$

The Euler–Lagrange equation for order parameter equilibrium (3.27) or (3.104) becomes

$$\tfrac{3}{4}\bar{l}\bar{\eta}'' - 12\eta(1 - 3\eta + 2\eta^2)/\bar{l} + \tfrac{1}{2}\bar{\gamma}_0(\bar{\gamma} - \bar{\gamma}_0\varphi)\varphi' = 0. \tag{3.109}$$

Solutions now depend on only two material parameters, dimensionless length ratio $\bar{l}$ and twinning eigen-shear $\bar{\gamma}_0$, when interpolation function $\varphi(\eta)$ is fully prescribed.

3.4.2. *Homogeneous elasticity and twinning*

Solutions to the problem outlined in Section 3.4.1 are now sought for which twinning is spatially homogeneous:

$$\eta(\bar{X}) = \eta_{\text{H}} = \text{constant}, \qquad \bar{\eta}'(\bar{X}) = \bar{\eta}''(\bar{X}) = 0. \tag{3.110}$$

A subset of this class of solutions is shown in Figure 1(b), for which the domain remains perfectly elastic and $\eta = 0 \forall \bar{X} \in [0, 1]$. Shear stress is constant by (3.108). Since $\varphi(\eta_{\text{H}}) = $ constant, it follows from (3.106) and (3.110) that strain $\bar{\gamma}$ is also constant:

$$\bar{P} = \bar{\gamma} - \bar{\gamma}_0\varphi(\eta_{\text{H}}) = \text{constant} \Rightarrow \bar{\gamma} = \bar{P} + \bar{\gamma}_0\varphi(\eta_{\text{H}}) = \text{constant}. \tag{3.111}$$

Let the domain be fixed at $\bar{X} = 0$, and denote by $\bar{v}$ the shear displacement at $\bar{X} = 1$:

$$\bar{v}(0) = 0, \qquad \bar{v}(1) = \bar{v} = \int_0^1 \bar{\gamma}d\bar{X} = \bar{\gamma}\int_0^1 d\bar{X} = \bar{\gamma}. \tag{3.112}$$

Using (3.110), order parameter equilibrium (3.109) requires

$$24\eta(1 - 3\eta + 2\eta^2) = \bar{l}\bar{\gamma}_0(\bar{\gamma} - \bar{\gamma}_0\varphi)\varphi'. \tag{3.113}$$

Further analysis requires selection of interpolation function $\varphi(\eta)$ first introduced in (2.5). Choosing $\varphi = 3\eta^2 - 2\eta^3$ from (2.35), equality (3.113) becomes the fifth-order polynomial expression

$$6\bar{\gamma}_0^2\eta^5 - 15\bar{\gamma}_0^2\eta^4 + \left(9\bar{\gamma}_0^2 + 24/\bar{l}\right)\eta^3 + (3\bar{\gamma}\bar{\gamma}_0 - 36/\bar{l})\eta^2 - (3\bar{\gamma}\bar{\gamma}_0 - 12/\bar{l})\eta = 0. \tag{3.114}$$

This polynomial has two imaginary roots and the three real roots listed below:

$$\eta_H = 0, \qquad \eta_H = 1, \qquad \eta_H = \frac{1}{2} + \frac{3a}{2d} + \frac{2b}{3d} + \frac{d}{6a}; \tag{3.115}$$

$$a = \bar{\gamma}_0^2, \qquad b = 12/\bar{l}, \qquad c = \bar{\gamma}\bar{\gamma}_0, \tag{3.116}$$

$$d = \{27a^3 - 54a^2c + 2\sqrt{a^3[16b^3 + 243a^2(b - 3c) - 27a(4b^2 - 27c^2)]}\}^{1/3}. \tag{3.117}$$

Numerical evaluation of the third solution in (3.115) over physically realistic ranges of parameters $10^{-5} \le \bar{l} \le 0.1$, $1 \le \bar{\gamma}_0 \le 10^3$, and $0 < \bar{\gamma} \le \bar{\gamma}_0$ produced no values within the constraints $\eta_H \in (0, 1)$. Thus, the only feasible homogeneous solutions are $\eta_H = 0$ and $\eta_H = 1$. (A recent computational phase field study of spinodal twinning [38], on the other hand, did find possible homogeneous solutions with uniform order parameter values in the range $0 < \eta_H < 1$, though governing and boundary conditions imposed in that work differ from those considered here.) The total energy functional (3.107) becomes

$$\bar{\Psi}(\bar{\upsilon}, \eta_H) = \int_0^1 \left[\tfrac{1}{4}(\bar{\gamma} - \bar{\gamma}_0\varphi)^2 + 6\eta_H^2(1 - \eta_H)^2/\bar{l} \right] d\bar{X}. \tag{3.118}$$

For $\eta_H = 0$ or $\eta_H = 1$, using (2.37) and noting here that $\bar{\gamma} = \bar{\upsilon}$,

$$\bar{\Psi}_E = \bar{\Psi}(\bar{\gamma}, 0) = \tfrac{1}{4}\bar{\gamma}^2, \qquad \bar{\Psi}_T = \bar{\Psi}(\bar{\gamma}, 1) = \tfrac{1}{4}(\bar{\gamma} - \bar{\gamma}_0)^2, \tag{3.119}$$

where $\bar{\Psi}_E$ is the energy of the elastic solution (no twin) and $\bar{\Psi}_T$ is the energy of the fully twinned homogeneous solution. These two energies are equal at $\bar{\gamma}/\bar{\gamma}_0 = \frac{1}{2}$, with the former purely elastic solution in Figure 1(b) energetically favorable for applied shear $\bar{\gamma}/\bar{\gamma}_0 < \frac{1}{2}$ and the latter fully twinned solution favourable for $\bar{\gamma}/\bar{\gamma}_0 > \frac{1}{2}$.

3.4.3. *Stability*

Stability, or lack thereof, of homogeneous purely elastic solution $\eta = \eta_H = 0$ is now analysed. Interpolation function $\varphi(\eta)$ is left general until the conclusion of the analysis.

A family of candidate solutions is now introduced, where α is a scalar parameter (i.e. perturbation) whose magnitude denotes deviation from the homogeneous solution η_H:

$$\eta = \eta(\bar{X}, \alpha), \quad \eta(\bar{X}, 0) = \eta_H = 0; \qquad \bar{\upsilon} = \bar{\upsilon}(\bar{X}, \alpha), \quad \bar{\gamma}(\bar{X}, \alpha) = \partial\bar{\upsilon}/\partial\bar{X}. \tag{3.120}$$

Displacement boundary conditions are imposed, and candidate solutions are required to obey the same such boundary conditions imposed for the homogeneous solution:

$$\bar{\upsilon}(0, \alpha) = \bar{\upsilon}(0, 0) = 0, \qquad \bar{\upsilon}(1, \alpha) = \bar{\upsilon}(1, 0) = \bar{\upsilon} = \int_0^1 \bar{\gamma}(\bar{X}, \alpha)d\bar{X}. \tag{3.121}$$

Candidate solutions for η are further expected to have vanishing order parameter gradients $\bar{\eta}' = \partial\eta(\bar{X}, \alpha)/\partial\bar{X}$ at the endpoints, as trivially satisfied by the homogeneous solution:

$$\bar{\eta}'(0, \alpha) = \bar{\eta}'(1, \alpha) = 0. \tag{3.122}$$

Define the following integral function of parameter α:

$$\vartheta(\alpha) = \int_0^1 \varphi d\bar{X}, \qquad \varphi = \varphi[\eta(\bar{X}, \alpha)], \qquad d\vartheta/d\alpha = \int_0^1 \varphi'(\partial\eta/\partial\alpha)d\bar{X}. \tag{3.123}$$

Recalling from (3.106) that shear stress obeys $\bar{P} = \bar{\gamma} - \bar{\gamma}_0 \varphi$ and is independent of $\bar{X}$,

$$\bar{\upsilon} = \int_0^1 \bar{\gamma}(\bar{X}, \alpha)\mathrm{d}\bar{X} = \bar{P}(\alpha) + \bar{\gamma}_0 \int_0^1 \varphi \mathrm{d}\bar{X} = \bar{P}(\alpha) + \bar{\gamma}_0 \vartheta(\alpha), \tag{3.124}$$

$$\bar{\gamma}(\bar{X}, \alpha) = \bar{P}(\alpha) + \bar{\gamma}_0 \varphi[\eta(\bar{X}, \alpha)] = \bar{\upsilon} + \bar{\gamma}_0(\varphi - \vartheta). \tag{3.125}$$

The total energy of (3.107) in terms of parameter α then follows as

$$\bar{\Psi}(\alpha) = \tfrac{1}{4} \int_0^1 (\bar{\upsilon}^2 - 2\bar{\upsilon}\bar{\gamma}_0 \varphi \vartheta + \bar{\gamma}_0^2 \vartheta^2)\mathrm{d}\bar{X} + 3 \int_0^1 [2\eta^2(1 - \eta)^2/\bar{l} + \tfrac{1}{8}\bar{l}(\eta')^2]\mathrm{d}\bar{X}. \tag{3.126}$$

The first variation of total energy is, upon integration by parts and use of boundary conditions in (3.122),

$$\delta\bar{\Psi}(\alpha) = \frac{1}{2} \int_0^1 \left[(\bar{\gamma}_0^2 \vartheta - \bar{\upsilon}\bar{\gamma}_0 \varphi)\frac{\mathrm{d}\vartheta}{\mathrm{d}\alpha} - \bar{\upsilon}\bar{\gamma}_0 \vartheta \varphi' \frac{\partial\eta}{\partial\alpha} \right]\mathrm{d}\bar{X}\delta\alpha$$
$$+ 3 \int_0^1 \left[\frac{4}{\bar{l}}\eta(1 - 3\eta^2 + 2\eta^3) - \frac{\bar{l}}{4}\bar{\eta}'' \right] \frac{\partial\eta}{\partial\alpha}\mathrm{d}\bar{X}\delta\alpha. \tag{3.127}$$

Noting for the homogeneous solution ($\alpha = 0$) that

$$\eta(\bar{X}, 0) = \bar{\eta}''(\bar{X}, 0) = 0, \qquad \vartheta = \varphi = 0, \qquad \mathrm{d}\vartheta/\mathrm{d}\alpha = \varphi'\partial\eta/\partial\alpha, \tag{3.128}$$

the first variation of total energy evaluated at $\alpha = 0$ vanishes, as it should for an equilibrium state:

$$\delta\bar{\Psi}(0) = 0. \tag{3.129}$$

The second variation of energy functional (3.126) at $\alpha = 0$ is computed upon successive differentiation as

$$\frac{\delta^2\bar{\Psi}}{\delta\alpha^2}(0) = \frac{1}{2}(\bar{\gamma}_0^2 - 2\bar{\upsilon}\bar{\gamma}_0)[\varphi'(0)]^2 \int_0^1 \left(\frac{\partial\eta}{\partial\alpha}\right)^2 \mathrm{d}\bar{X} + \frac{12}{\bar{l}} \int_0^1 \left(\frac{\partial\eta}{\partial\alpha}\right)^2 \mathrm{d}\bar{X}$$
$$+ \frac{3\bar{l}}{4} \int_0^1 \left(\frac{\partial\bar{\eta}'}{\partial\alpha}\right)^2 \mathrm{d}\bar{X}. \tag{3.130}$$

Noting that the rightmost term of (3.130) is always nonnegative, and noting that for the homogeneous solution that $\bar{\upsilon} = \bar{\gamma}$, a lower bound for the unstable domain in terms of applied shear strain is determined by the sum of coefficients of the first two integrals on the right of (3.130):

$$\bar{\gamma} > \frac{\bar{\gamma}_0}{2} + \frac{12}{\bar{l}\bar{\gamma}_0[\varphi'(0)]^2}. \tag{3.131}$$

If $\varphi'(0) = 0$, as occurs in (2.37) for particular choice (2.35) considered in Section 3.4.2, the homogeneous elastic solution is stable with respect to perturbation α (i.e. $\frac{\delta^2\bar{\Psi}}{\delta\alpha^2}(0) > 0$) for any applied strain since $\bar{l} > 0$. Even if stable in the above sense, such an elastic solution may reflect a local minimum energy configuration (i.e. metastability), since other solutions (e.g. a heterogeneous η field or fully twinned with $\eta_H = 1$) may have lower total energy at the same imposed $\bar{\upsilon}$. For a linear interpolator (e.g. $\varphi = \eta$) similar to that considered in [40], stability of the homogeneous elastic solution is not always ensured for $\bar{\gamma}/\bar{\gamma}_0 > \frac{1}{2}$.

3.4.4. *Localized complete twinning*

Considered next is the problem of Figure 1(c): a stress-free domain with localized twinning at its midpoint. Applied displacement $\bar{v} = \bar{v}(1)$ takes a value within $0 < \bar{v} < \bar{\gamma}_0$. Mechanical loading conditions are

$$\bar{P} = \bar{\gamma}(\bar{X}) - \bar{\gamma}_0 \varphi[\eta(\bar{X})] = 0 \Rightarrow \bar{\gamma} = \bar{\gamma}_0 \varphi, \qquad \bar{v}(0) = 0. \tag{3.132}$$

Boundary and symmetry conditions on the order parameter are

$$\bar{\eta}'(0) = \bar{\eta}'(1) = 0, \qquad \eta\left(\tfrac{1}{2}\right) = 1, \qquad \eta\left(\tfrac{1}{2} - \bar{X}\right) = \eta\left(\tfrac{1}{2} + \bar{X}\right). \tag{3.133}$$

Vanishing order parameter gradients at the endpoints corresponds to $r = 0$ in (2.15) and (2.19). Order parameter equilibrium (3.109) can be written as

$$\tfrac{3}{4}\bar{l}\bar{\eta}'' + \tfrac{1}{2}\bar{P}\bar{\gamma}_0\varphi' - (24/\bar{l})\eta^3 + (36/\bar{l})\eta^2 - (12/\bar{l})\eta = 0. \tag{3.134}$$

Substituting the null stress condition (3.132), this becomes the nonlinear second-order differential equation

$$\bar{\eta}'' - (32/\bar{l}^2)\eta^3 + (48/\bar{l}^2)\eta^2 - (16/\bar{l}^2)\eta = 0. \tag{3.135}$$

Notice that for null shear stress, the particular choice of function φ becomes irrelevant. Differential equation (3.135) can be written as

$$\frac{\mathrm{d}}{\mathrm{d}\eta}[(\bar{\eta}')^2] = \frac{16}{\bar{l}^2}\frac{\mathrm{d}}{\mathrm{d}\eta}[\eta^2(1-\eta)^2]. \tag{3.136}$$

Integrating both sides of (3.136) from the left side of the domain where $\eta(\bar{X}) = \eta(0) = 0$ to any η at point $\bar{X} \leq \tfrac{1}{2}$ and taking the positive root gives the first-order nonlinear differential equation

$$\mathrm{d}\eta/\mathrm{d}\bar{X} = 4\eta(1-\eta)/\bar{l}. \tag{3.137}$$

Inversion of this equation and integration produce

$$\bar{X}(\eta) = \bar{l}\int_0^1 \mathrm{d}\eta/[4\eta(1-\eta)]. \tag{3.138}$$

Integral (3.138) is evaluated numerically (here via trapezoidal quadrature) and then inverted to give order parameter profile $\eta(\bar{X})$ over the left half of the domain, i.e. over $0 \leq \bar{X} \leq \tfrac{1}{2}$. Points $\bar{X}_1$ and $\bar{X}_2$ bounding the region where $0 < \eta < 1$ are determined simultaneously by the condition $\eta = 1 \forall \bar{X} \in (\bar{X}_2, \tfrac{1}{2}]$ and the magnitude of applied shear that sets the width of the fully twinned region:

$$\bar{v} = \int_{\bar{X}_1}^{\bar{X}_2} \bar{\gamma}\mathrm{d}\bar{X} + \bar{\gamma}_0(1 - 2\bar{X}_2). \tag{3.139}$$

The order parameter profile for the right half of the domain can be constructed using symmetry conditions in (3.133). Shown in Figure 5(a) is the order parameter profile for applied displacement $\bar{v} = \bar{\gamma}_0/2$. The domain shown is limited to the relatively small region where η varies with $\bar{X}$. For example, for $\bar{l} = 0.01$, $\bar{X}_1 \approx 0.22$ and $\bar{X}_2 \approx 0.24$. The width of the twin boundary region $\bar{X}_2 - \bar{X}_1$ increases with increasing $\bar{l}$.
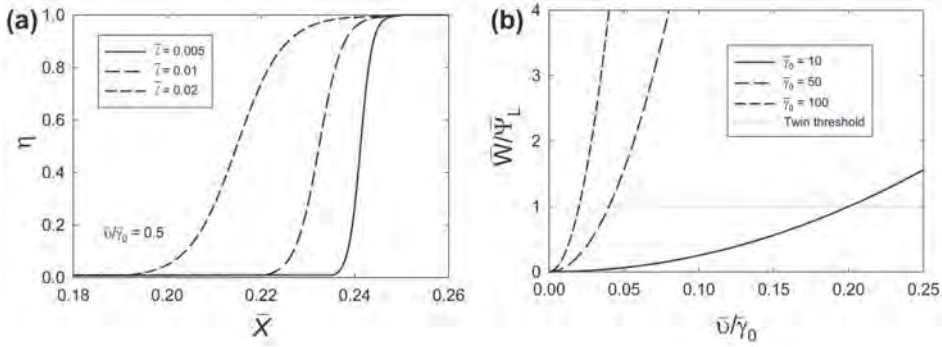
Figure 5. Inhomogeneous numerical solution (a) for stress-free twinning at applied dimensionless shear displacement of $\bar{\upsilon} = \bar{\gamma}_0/2$: profile of order parameter η at the left twin boundary. Dimensionless coordinate is $\bar{X}$; dimensionless characteristic length is $\bar{l}$; normalized complete twinning shear is $\bar{\gamma}_0$. Ratio (b) of homogeneous elastic energy $\bar{W}$ to localized stress-free twinning energy $\bar{\Psi}_L$ vs. applied normalized shear $\bar{\upsilon}/\bar{\gamma}_0$. Transition from homogeneous elasticity to localized stress-free twinning is energetically favourable if $\bar{W}/\bar{\Psi}_L > 1$.

The total energy of the localized stress-free solution is found by application of (3.107), which reduces here via (3.132) (yielding strain energy $\bar{W} = 0$ from $\bar{P} = 0$) and (3.137) to

$$\bar{\Psi}_L = 2\int_0^{1/2}\{6\eta^2(1-\eta)^2/\bar{l} + \tfrac{3}{8}\bar{l}[4\eta(1-\eta)/\bar{l}]^2\}d\bar{X} = (24/\bar{l})\int_{\bar{X}_1}^{\bar{X}_2}\eta^2(1-\eta)^2 d\bar{X} = 1. \tag{3.140}$$

The final value $\bar{\Psi}_L = 1$ is consistent with normalization (3.105) giving $\Psi_L = 2\Gamma/L$ (i.e. the exact surface energy of two unstressed twin boundaries) and was verified numerically for $10^{-6} \le \bar{l} \le 0.2$. Shown in Figure 5(b) is total energy for the homogeneous elastic solution of (3.119) of Section 3.4.2, $\bar{W} = \bar{\Psi}_E = \tfrac{1}{4}\bar{\gamma}^2$ normalized by $\bar{\Psi}_L = 1$. Localized stress-free twinning under displacement control (Figure 1(c)) becomes energetically favourable to homogeneous elasticity (Figure 1(b)) when $\bar{\upsilon}$ is large enough such that $\bar{W} > 1 \Leftrightarrow \bar{\Psi}_E > \bar{\Psi}_L \Leftrightarrow \bar{\gamma} > 2$. The larger the value of $\bar{\gamma}_0$, the greater elastic energy relieved by twinning at a given value of $\bar{\upsilon}/\gamma_0$.

Solution of a more complex boundary value problem involving nonzero shear stress $\bar{P}$ and heterogeneous or localized twinning corresponds to solution of (3.134) with appropriate boundary conditions and requires choice of interpolation function φ. Solution of this more difficult differential equation should be possible, but requires more advanced numerical methods beyond the present scope.

Verification is straightforward that this candidate solution involving stress-free, localized twinning, in the absence of fracture, is valid for the fully coupled theory of Section 3.2. Since $\xi(\bar{X}) = 0$, $\bar{P} = \bar{\gamma} - \bar{\gamma}_0 = 0 \Rightarrow \bar{\gamma} = \bar{\gamma}_0\varphi$. Fracture order parameter equilibrium (3.26) requires

$$\hat{\imath}'(0)R[\tfrac{3}{8}\bar{l}(\eta')^2 + 6\eta^2(1-\eta)^2/\bar{l}] = 0. \tag{3.141}$$

This equation can be satisfied unconditionally by choosing a degradation function satisfying $\hat{\imath}'(0) = 0$; for example, a possible choice also obeying requirements in (2.29) is $\hat{\imath}(\xi) = 1 - \varphi(\xi) = 1 - \eta^2(3 - 2\eta)$. An even simpler example is $\hat{\imath} = 1$, which decouples energies of twin boundaries and fracture surfaces. Twinning order parameter equilibrium (3.27) requires

$$\hat{\iota}(0)R[\tfrac{3}{4}\bar{l}\bar{\eta}'' - 12\eta(1 - 3\eta + 2\eta^2)/\bar{l}] = 0, \tag{3.142}$$

which is identical to (3.135) for finite $R = \Gamma/\Upsilon$ since $\hat{\iota}(0) = 1$ by (2.29). Therefore, it follows that this solution, depicted in Figure 1(c), is admissible in the fully coupled theory so long as $\hat{\iota}$ is chosen appropriately. Choosing $\hat{\iota}(\xi) = \hat{\phi}(\xi)$ is incompatible with such a solution since then $\hat{\iota}' = 2(\xi - 1)$ and (3.141) is no longer satisfied, in general, for nonzero R.

4. Model predictions for real crystalline solids

Upon consideration of stabilities and total energies of various solutions derived in Section 3 for the phase field constitutive model of Section 2 applied to a finite simple shear problem, various criteria for shear-induced fracture and twinning can be deduced. These criteria can be applied to real materials by converting normalized quantities to their dimensional forms, as demonstrated next.

First consider mode II fracture. The shear stress at which a homogeneously damaged solid becomes unstable according to (3.63) and (3.79) is converted to dimensional form via (3.19), leading to

$$P_C = \tfrac{3}{16}\sqrt{6\mu_0\Upsilon/l}. \tag{4.1}$$

The shear stress at which localized fracture becomes energetically favourable to homogeneous elastic deformation is found according to derivations in Section 3.3.4 and listed in (3.47):

$$P_F = 2\sqrt{\mu_0\Upsilon/L} \quad \text{for } l \lesssim 0.01L. \tag{4.2}$$

These two criteria for shear fracture can be compared with the so-called theoretical fracture strength [3,44,46] needed to relatively displace (here under shear loading) two slabs of linear elastic material here by a slip distance equal to the spacing between interatomic planes:

$$P_{\text{th, frac}} = \mu_0/(2\pi). \tag{4.3}$$

Unlike theoretical strength (4.3), which depends only on shear modulus, the new criteria presented in (4.1) and (4.2) are proportional to the square root of the product of shear modulus and surface energy.

Distinctions and similarities among the fracture criteria discussed above and Griffith's criterion [67] are noteworthy. Under plane strain conditions, in the context of pure mode II loading, Griffith's criterion for extension of a straight crack of length $2a$ in an infinite isotropic linear elastic medium can be stated as [43]

$$P_G = 2\sqrt{\mu_0\Upsilon/[(1 - \nu)\pi a]}, \tag{4.4}$$

with P_G the far-field shear stress and ν Poisson's ratio. Griffith's criterion (4.4) applies for a pre-existing sharp crack of finite length in an infinite body, while (4.1)–(4.3) correspond to nucleation of a crack in an initially homogeneous crystal of finite size. While (4.1), (4.2) and (4.4) all incorporate a shear modulus and surface energy, only the latter (Griffith) also involves compressibility via Poisson's ratio. Note also that (4.2) and (4.4) give identical predictions when domain size $L = (1 - \nu)\pi a \approx 2a$. Griffith's criterion can be extended for applications to bodies of finite size by accounting for dependence of the crack tip stress intensity factor on geometry of the body, in which case the critical far-field stress for crack

extension depends on both the initial crack length and the position of the crack relative to external surfaces of the body.

It is emphasized that all fracture criteria considered thus far apply for brittle elastic solids. When crack tip plasticity becomes important, an approximate and simple way of considering the corresponding increase in toughness involves replacement of surface energy Υ in the above criteria with an effective (increased) surface energy accounting for plastic work in the process zone [68]. A more physically detailed and complete model for ductile crystals would involve including additional order parameters (and their corresponding effects on kinematics and energy) in the phase field framework accounting for slip of full and/or partial dislocations on each relevant slip system [37,69].

Next, consider deformation twinning. The shear stress at which localized twinning becomes energetically favourable to homogeneous elastic deformation is found according to derivations in Section 3.4.4 and listed in (3.46):

$$P_{\mathrm{T}} = 2\sqrt{R}\sqrt{\mu_0 \Upsilon / L} = 2\sqrt{\mu_0 \Gamma / L}. \tag{4.5}$$

This new criterion, like those above for fracture, is proportional to the square root of the product of a shear modulus and a surface energy. Criterion (4.5) can be compared with two others from the literature, the theoretical strength associated with twinning [70,71]:

$$P_{\mathrm{th, \, twin}} = \mu_0 \gamma_0 / (2\pi). \tag{4.6}$$

and the twinning stress associated with moving a partial twinning dislocation of Burgers magnitude b_{P} against the resistance associated with stacking fault energy $W_{\mathrm{SF}} \approx 2\Gamma$ [3,46]:

$$P_{\mathrm{SF, \, twin}} = 2\Gamma / b_{\mathrm{P}}. \tag{4.7}$$

Representative properties for a generic material of the sort considered most often in derivations of Section 3 as well as for three real materials–sapphire, calcite and magnesium– are listed in Table 2. Properties of the real crystalline solids are obtained from [5,8,39] and references quoted therein, with the exception of cohesive surface energy for magnesium [72] and b_{P}, the latter which is necessarily obtained from additional references for sapphire [50], calcite [4] and magnesium [73].

Each of these crystals exhibits multiple twin systems in nature. Considered here are twinning on the rhombohedral (R) and basal (B) systems in sapphire, respectively $\langle 1\,\bar{1}\,0\,\bar{1}\rangle$ $\{1\,\bar{1}\,0\,2\}$ and $\langle 1\,\bar{1}\,0\,0\rangle\{0\,0\,0\,1\}$ in hexagonal Miller indices. The e^+ twin system in calcite corresponds to $\langle 0\,0\,1\rangle\{1\,1\,0\}$ in the cleavage rhomobohedral pseudocell [39,42]. The primary tensile twin system in magnesium corresponds to $\langle 1\,0\,\bar{1}\,1\rangle\{\bar{1}012\}$ in hexagonal Miller indices [8].

Criteria (4.1), (4.2) and (4.5) depend on a length parameter (l or L), with strength increasing as size decreases in an inverse square-root manner, a phenomenon widely observed in materials science (e.g. the Hall–Petch effect [74]). In the analysis that follows next, $l = 1$nm is chosen, consistent with prior phase field studies of structural transformations [5,8,9,39]. This length corresponds physically to the distance from an externally unstressed fracture surface or twin boundary within which atoms in a crystal deviate from their ideal static positions. Also, $\bar{l} = 0.01$ is regarded as fixed for consistency with results of the study of a generic solid considered most often earlier in this paper. These choices lead to a representative domain size of $L = 0.1\,\mu$m for a material element containing a single localized fracture or fully twinned zone. The present analysis precludes plastic

Table 2. Material properties ($l = 1$nm, $\bar{l} = 0.01$).

Material	μ_0 (GPa)	Υ [J/m^2]	Γ [J/m^2]	R	γ_0	$\bar{\gamma}_0$	b_P [nm]
Generic	100	1	1	1	0.5	50	0.1
Sapphire (R twin)	167	6	0.125	0.021	0.202	73.8	0.071
Sapphire (B twin)	167	40	0.745	0.019	0.635	95.1	0.274
Calcite (e^+ twin)	36.7	0.347	0.183	0.527	0.694	98.3	0.130
Magnesium (tensile)	19.0	1.5	0.117	0.078	0.130	16.6	0.049

Table 3. Model predictions and comparisons for real crystals (GPa).

Material	P_C	P_F	$P_{\text{th, frac}}$	Frac. data [ref]	P_L	$P_{\text{th, twin}}$	$P_{\text{SF, twin}}$	Twin data [ref]
Generic	4.6	2.0	15.9	–	2.0	8.0	20	–
Sapphire (R)	14.5	6.3	26.6	7.9 [50]	0.91	5.4	3.5	1.0 [50]
Sapphire (B)	37.5	16.3	26.6	–	2.23	16.9	5.4	4.0 [50]
Calcite	1.6	0.71	5.8	–	0.52	4.1	2.8	10^{-3} [42]
Magnesium	2.5	1.1	3.0	–	0.30	0.39	4.8	0.08 [76]

deformation in the form of conventional slip of dislocations that might occur (e.g. in ductile metal crystals); to address this, the kinematic framework of Section 2.1 should be extended to account for dislocation glide and stored defect content [75], as should the governing equations of the phase field theory [37,69]. Although dislocation slip and deformation twinning are often competing mechanisms, omission of plastic flow is deemed reasonable in the present application since twinning is much easier than slip in calcite [42], rhombohedral twinning is preferred over pyramidal slip in sapphire [50] and tensile twinning is preferred over pyramidal slip in magnesium [41].

Predictions of criteria (4.1)–(4.7) are compared in Table 3. Also listed are data from other sources. For sapphire, shear stress data for fracture resistance on R planes and twinning resistance on B and R systems are obtained from nonlinear thermoelastic analysis of shear strengths observed in shock physics experiments [50]. Data on twinning resistance for calcite is obtained from direct shear experiments [42]; however, this stress as reported may underestimate the true twinning resistance since it is an average value for the entire specimen that omits the effect of local stress concentrations near the twin nucleus. Data on twinning resistance for magnesium is obtained from atomic simulations [76]. First examining fracture results, Table 3 shows that $P_C > P_F$ for all considered twin systems of all materials, and that P_F provides closest agreement with the test datum on sapphire, with P_C and $P_{\text{th, frac}}$ greatly overestimating fracture strength. Next examining twinning results, it is observed that $P_L < P_{\text{th, twin}}$ and $P_L < P_{\text{SF, twin}}$ for all materials. For R twinning in sapphire and for twinning in calcite and magnesium, P_L is closer than the other two criteria to the test data; for B twinning in sapphire, P_L and $P_{\text{SF, twin}}$ are of comparable accuracy relative to the datum.

5. Conclusions

A continuum phase field theory for fracture and deformation twinning has been developed. Key features of the theory include assignment of distinct order parameters for fracture and twinning behaviours, treatment of finite deformation and nonlinear elastic response, and degradation of elastic strain energy and twin boundary energy with cumulative damage. The present paper reports the first known model accounting for all such features. Outcomes of the model have been analysed for an element of material undergoing simple shear deformation. Analytical and/or numerical solutions have been obtained for scenarios involving isolated physical mechanisms depicted by the model, including homogeneous elasticity, homogeneous damage, localized fracture and localized twinning. In addition to providing immediate insight into pure shear behaviour, these solutions can be used later for verification of more advanced numerical methods to eventually be applied towards more complex boundary value problems. Stable domains of homogeneous solutions have been identified, extending previous derivations that only addressed linear elastic behaviour and tensile deformations. Coupled fracture and twinning mechanisms have also been considered. Criteria for shear stresses leading to fracture and twinning have been derived and evaluated for several real materials: sapphire, calcite and magnesium. These criteria have been shown to usually demonstrate closer agreement with available test data than do simple criteria based on the concept of theoretical strength.

Disclosure statement

No potential conflict of interest was reported by the authors.

References

[1] R.A. Schultz, M.C. Jensen and R.C. Bradt, Int. J. Fracture 65 (1994) p.291.
[2] J.W. Christian and S. Mahajan, Prog. Mater. Sci. 39 (1995) p.1.
[3] J.D. Clayton, *Nonlinear Mechanics of Crystals*, Springer, Dordrecht, 2011.
[4] V.S. Boiko, R.I. Garber and A.M. Kosevich, *Reversible Crystal Plasticity*, AIP Press, New York, 1994.
[5] J.D. Clayton and J. Knap, Acta Mater. 61 (2013) p.5341.
[6] F.D. Fischer, E.R. Oberaigner and T. Waitz, Scripta Mater. 61 (2009) p.959.
[7] E.B. Tadmor and S. Hai, J. Mech. Phys. Solids 51 (2003) p.765.
[8] J.D. Clayton and J. Knap, Physica D 240 (2011) p.841.
[9] V.A. Levitas, V.A. Levin, K.M. Zingerman and E.I. Freiman, Phys. Rev. Lett. 103 (2009) p.025702.
[10] B. Bourdin, G.A. Francfort and J.J. Marigo, J. Mech. Phys. Solids 48 (2000) p.797.
[11] B. Bourdin, G.A. Francfort and J.J. Marigo, J. Elasticity 91 (2008) p.5.
[12] G. Del Piero, G. Lancioni and R. March, J. Mech. Phys. Solids 55 (2007) p.2513.
[13] I.S. Aranson, V.A. Kalatsky and V.M. Vinokur, Phys. Rev. Lett. 85 (2000) p.118.
[14] M.J. Borden, C.V. Verhoosel, M.A. Scott, T.J.R. Hughes and C.M. Landis, Comput. Meth. Appl. Mech. Eng. 217 (2012) p.77.
[15] J.D. Clayton and J. Knap, Int. J. Fracture 189 (2014) p.139.
[16] V. Hakim and A. Karma, Phys. Rev. Lett. 95 (2005) p.235501.
[17] V. Hakim and A. Karma, J. Mech. Phys. Solids 57 (2009) p.342.
[18] Y.M. Jin, Y.U. Wang and A.G. Khachaturyan, Appl. Phys. Lett. 79 (2001) p.3071.
[19] A. Karma, D.A. Kessler and H. Levine, Phys. Rev. Lett. 87 (2001) p.045501.

[20] C. Kuhn and R. Müller, Eng. Frac. Mech. 77 (2010) p.3625.
[21] V.I. Marconi and A. Jagla, Phys. Rev. E 71 (2005) p.036110.
[22] C. Miehe, F. Welschinger and M. Hofacker, Int. J. Numer. Meth. Eng. 83 (2010) p.1273.
[23] R. Spatschek, E. Brener and A. Karma, Philos. Mag. 91 (2011) p.75.
[24] G.Z. Voyiadjis and N. Mozaffari, Int. J. Solids Structures 50 (2013) p.3136.
[25] H. Amor, J.-J. Marigo and C. Maurini, J. Mech. Phys. Solids 57 (2009) p.1209.
[26] A. Abdollahi and I. Arias, Acta Mater. 59 (2011) p.4733.
[27] A. Abdollahi and I. Arias, Modelling Simul. Mater. Sci. Eng. 19 (2011) p.074010.
[28] A. Abdollahi and I. Arias, Int. J. Fracture 174 (2012) p.3.
[29] B.-X. Xu, D. Schrade, D. Gross and R. Mueller, Int. J. Fracture 166 (2010) p.163.
[30] A. Benallal and J.-J. Marigo, Modelling Simul. Mater. Sci. Eng. 15 (2007) p.S283.
[31] C. Kuhn, *Numerical and analytical investigation of a phase field model for fracture*, Ph.D. thesis, Tech. Univ. Kaiserslautern, 2013.
[32] C. Kuhn and R. Müller, Proc. Appl. Math. Mech. 12 (2012) p.161.
[33] C. Kuhn and R. Müller, *Crack nucleation in phase field fracture models*, in *Proceedings of the 13th International Congress on Fracture*, Beijing, China, 2013.
[34] K. Pham, H. Amor, J.-J. Marigo and C. Maurini, Int. J. Damage Mech. 20 (2011) p.618.
[35] K. Pham, J.-J. Marigo and C. Maurini, J. Mech. Phys. Solids 59 (2011) p.1163.
[36] T.W. Heo, Y. Wang, S. Bhattacharya, X. Sun, S. Hu and L.Q. Chen, Philos. Mag. Lett. 91 (2011) p.110.
[37] S.Y. Hu, C.H. Henager and L.-Q. Chen, Acta Mater. 58 (2010) p.6554.
[38] T.W. Heo, Y. Wang and L.-Q. Chen, Philos. Mag. 94 (2014) p.888.
[39] J.D. Clayton and J. Knap, Modelling Simul. Mater. Sci. Eng. 19 (2011) p.085005.
[40] F.E. Hildebrand and C. Miehe, Philos. Mag. 92 (2012) p.4250.
[41] A. Staroselsky and L. Anand, Int. J. Plasticity 19 (2003) p.1843.
[42] H. Kaga and J.J. Gilman, J. Appl. Phys. 40 (1969) p.3196.
[43] S.A. Meguid, *Engineering Fracture Mechanics*, Elsevier, London, 1989.
[44] J. Frenkel, Z. Phys. 37 (1926) p.572.
[45] W.R. Tyson, Philos. Mag. 14 (1966) p.925.
[46] J.P. Hirth and J. Lothe, *Theory of Dislocations*, 2nd ed., Wiley, New York, 1982.
[47] R.A. Graham and W.P. Brooks, J. Phys. Chem. Solids 32 (1971) p.2311.
[48] D.E. Grady, Mech. Mater. 29 (1998) p.181.
[49] D.R. Curran, L. Seaman, T. Cooper and D.A. Shockey, Int. J. Impact Eng. 13 (1993) p.53.
[50] J.D. Clayton, Proc. R. Soc. Lond. A 465 (2009) p.307.
[51] R. Schmitt, C. Kuhn, R. Skorupski, M. Smaga, D. Eifler and R. Müller, Arch. Appl. Mech. (in press, 2014). doi:10.1007/s00419-014-0945-8.
[52] J.D. Clayton, Math. Mech. Solids 17 (2012) p.702.
[53] J.D. Clayton, *Differential Geometry and Kinematics of Continua*, World Scientific, Singapore, 2014.
[54] J.D. Clayton and D.L. McDowell, Int. J. Solids Structures 40 (2003) p.5669.
[55] J.D. Clayton and D.L. McDowell, Mech. Mater. 36 (2004) p.799.
[56] J.D. Clayton, Int. J. Fracture 163 (2010) p.151.
[57] J.D. Clayton, Philos. Mag. 92 (2012) p.2860.
[58] J.D. Clayton and K.M. Bliss, Mech. Mater. 68 (2014) p.104.
[59] J.D. Clayton, J. Mech. Phys. Solids 61 (2013) p.1983.
[60] J.D. Clayton, Int. J. Appl. Mech. 6 (2014) p.1450048.
[61] J.D. Clayton, Int. J. Eng. Sci. 79 (2014) p.1.
[62] K. Bhattacharya, Cont. Mech. Thermodyn. 5 (1993) p.205.
[63] S.M. Allen and J.W. Cahn, Acta Metall. 27 (1979) p.1085.
[64] H. Emmerich, *The Diffuse Interface Approach in Materials Science: Thermodynamic Concepts and Applications of Phase-field Models*, Springer, Berlin, 2003.

[65] B. Bourdin, J.-J. Marigo, C. Maurini and P. Sicsic, Phys. Rev. Lett. 112 (2014) p.014301.

[66] M. Hofacker and C. Miehe, Int. J. Fracture 178 (2012) p.113.

[67] A.A. Griffith, The theory of rupture, in *Proceedings of International Congress Applied Mechanics*, Delft, 1924, pp. 55–62.

[68] J.R. Rice and J.-S. Wang, Mater. Sci. Eng. A 107 (1989) p.23.

[69] M. Koslowski and M. Ortiz, Modelling Simul. Mater. Sci. Eng. 12 (2004) p.1087.

[70] R.L. Bell and R.W. Cahn, Proc. R. Soc. Lond. A 239 (1957) p.494.

[71] A.T. Paxton, P. Gumbsch and M. Methfessel, Philos. Mag. Lett. 63 (1991) p.267.

[72] A.E. Smith, Surf. Sci. 601 (2007) p.5762.

[73] J. Wang, R.G. Hoagland, J.P. Hirth, L. Capolungo, I.J. Beyerlein and C.N. Tomé, Scripta Mater. 61 (2009) p.903.

[74] R.W. Armstrong, Acta Mech. 225 (2014) p.1013.

[75] J.D. Clayton, D.J. Bammann and D.L. McDowell, Philos. Mag. 85 (2005) p.3983.

[76] A. Serra and D.J. Bacon, Philos. Mag. A 63 (1991) p.1001.

INTENTIONALLY LEFT BLANK.